Article

Cell Chemical Biology

Blockade of Oncogenic NOTCH1 with the SERCA Inhibitor CAD204520 in T Cell Acute Lymphoblastic Leukemia

Graphical Abstract

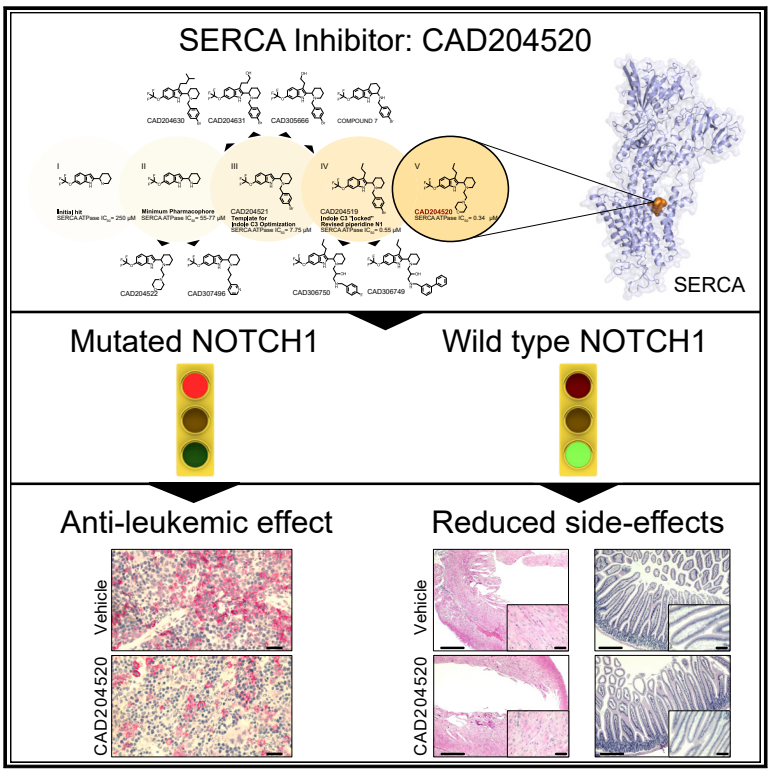

Highlights

- Identification of CAD204520, a highly selective SERCA inhibitor
- Crystal structure of CAD204520 in complex with SERCA
- CAD204520 inhibits HD and PEST *NOTCH1* mutations in lymphoid malignancies
- SERCA inhibition can be achieved *in vivo* without cardiac toxicity

Authors

Matteo Marchesini, Andrea Gherli, Anna Montanaro, ..., Maike Bublitz, William Dalby-Brown, Giovanni Roti

Correspondence

giovanni.roti@unipr.it

In Brief

Clinical translation of SERCA inhibitors has been hampered by the risk of adverse cardiac events. In this work, Marchesini and Gherli et al. identified a tolerable oral available SERCA inhibitor, CAD204520, and showed that modulation of clinically relevant NOTCH1 mutations in T cell acute lymphoblastic leukemia and mantle cell lymphoma.

Marchesini et al., 2020, Cell Chemical Biology *27*, 1–20
June 18, 2020
https://doi.org/10.1016/j.chembiol.2020.04.002

CellPress

Please cite this article in press as: Marchesini et al., Blockade of Oncogenic NOTCH1 with the SERCA Inhibitor CAD204520 in T Cell Acute Lymphoblastic Leukemia, Cell Chemical Biology (2020), https://doi.org/10.1016/j.chembiol.2020.04.002

Cell Chemical Biology
Article

CellPress

Blockade of Oncogenic NOTCH1 with the SERCA Inhibitor CAD204520 in T Cell Acute Lymphoblastic Leukemia

Matteo Marchesini,[1,10] Andrea Gherli,[1,10] Anna Montanaro,[1] Laura Patrizi,[2] Claudia Sorrentino,[1] Luca Pagliaro,[1] Chiara Rompietti,[2] Samuel Kitara,[3] Sabine Heit,[4] Claus E. Olesen,[5] Jesper V. Møller,[5] Monia Savi,[6] Leonardo Bocchi,[6] Rocchina Vilella,[6] Federica Rizzi,[1,7] Marilena Baglione,[1] Giorgia Rastelli,[1] Caterina Loiacono,[1] Roberta La Starza,[2] Cristina Mecucci,[2] Kimberly Stegmaier,[3,8] Franco Aversa,[1] Donatella Stilli,[6] Anne-Marie Lund Winther,[9] Paolo Sportoletti,[2] Maike Bublitz,[4] William Dalby-Brown,[9] and Giovanni Roti[1,11,*]

[1]University of Parma, Department of Medicine and Surgery, Parma 43126, Italy
[2]University of Perugia, Department of Medicine, Hematology and Clinical Immunology, Perugia 06123, Italy
[3]Department of Pediatric Oncology, Dana-Farber Cancer Institute, Harvard Medical School, Boston, MA 02215, USA
[4]University of Oxford, Department of Biochemistry, Oxford OX1 3QU, UK
[5]Aarhus University, Department of Biomedicine, 8000 Aarhus C, Denmark
[6]University of Parma, Department of Chemistry, Life Sciences and Environmental Sustainability, Parma 43124, Italy
[7]INBB – Biostructures and Biosystems National Institute, Rome 00136, Italy
[8]The Broad Institute, Cambridge, MA 02142, USA
[9]Cado Biotechnology IvS, Copenhagen, Denmark
[10]These authors contributed equally
[11]Lead Contact
*Correspondence: giovanni.roti@unipr.it
https://doi.org/10.1016/j.chembiol.2020.04.002

SUMMARY

The identification of SERCA (sarco/endoplasmic reticulum calcium ATPase) as a target for modulating gain-of-function *NOTCH1* mutations in Notch-dependent cancers has spurred the development of this compound class for cancer therapeutics. Despite the innate toxicity challenge associated with SERCA inhibition, we identified CAD204520, a small molecule with better drug-like properties and reduced off-target Ca^{2+} toxicity compared with the SERCA inhibitor thapsigargin. In this work, we describe the properties and complex structure of CAD204520 and show that CAD204520 preferentially targets mutated over wild-type NOTCH1 proteins in T cell acute lymphoblastic leukemia (T-ALL) and mantle cell lymphoma (MCL). Uniquely among SERCA inhibitors, CAD204520 suppresses *NOTCH1*-mutated leukemic cells in a T-ALL xenografted model without causing cardiac toxicity. This study supports the development of SERCA inhibitors for Notch-dependent cancers and extends their application to cases with isolated mutations in the PEST degradation domain of *NOTCH1*, such as MCL or chronic lymphocytic leukemia (CLL).

INTRODUCTION

Genetic alterations in Notch signaling have been described in the majority of human cancers (Lawrence et al., 2014). Most of the recurrent somatic mutations of NOTCH proteins (I–IV) are observed in the *NOTCH1* gene. *NOTCH1* encodes a single-pass transmembrane protein with transcription factor activity that acts in stem cell differentiation (Artavanis-Tsakonas et al., 1999; Pui et al., 1999), cell fate determination (Pui et al., 1999), and in tissue development processes (Penton et al., 2012). The NOTCH1 protein has several functional domains organized in evolutionarily conserved modules. The extracellular N-terminal domain is responsible for ligand binding through EGF-like calcium (Ca^{2+}-dependent repeats), which are followed by three LNR modules that protect the extracellular portion from cleavage in the absence of ligand. The heterodimerization domain (HD) is a linker between the extracellular tail and the intracellular NOTCH active form (ICN1). Notch1 activation requires two sequential protein cleavage steps mediated by ADAM10/17 metalloproteases and the presenilin-γ-secretase complex to release the intracellular portion of NOTCH1, ICN1, which translocates into the nucleus and mediates the activation of the Notch pathway (De Strooper et al., 1999; Kopan and Ilagan, 2009).

The involvement of NOTCH1 in the pathogenesis of T cell acute lymphoblastic leukemia (T-ALL), an aggressive form of leukemia that mainly affects children, was initially discovered in 1991 (Ellisen et al., 1991). Ellisen et al. (1991) described a chromosome translocation, t(7; 9), that juxtaposes the promoter elements of the T cell receptor-β (TCRB) to the 3′ end portion of the *NOTCH1* gene encoding its intracellular domain ICN1. This fusion results in the overexpression of ICN1 causing the activation of genes that promote T cell leukemogenesis. Similarly, activating *NOTCH1* mutations generate ligand-independent or proteasome-resistant ICN1 polypeptides that sustain T cell transformation and leukemia growth (Aster et al., 2008; Weng et al., 2004).

Although the frequency of mutations is highest in T-ALL, *NOTCH1* has emerged as one of the most frequently mutated

genes (~5%–20%) in chronic lymphocytic leukemia (CLL) (Di Ianni et al., 2009; Puente et al., 2011). The most frequent mutation, ~80%, is a 2-bp deletion in exon 34 that generates a premature stop codon (P2514fs*4) leading to a truncation of the C-terminal PEST region. As in T-ALL, these mutations cause an over-activation of Notch1 signaling because of the lack of its degradation (Arruga et al., 2014). Interestingly, additional studies reported a similar pattern of PEST mutations in mantle cell lymphoma (MCL) (Bea et al., 2013; Kridel et al., 2012) and in activated B cell-like (ABC) diffuse large B cell lymphoma (6.1%) (Schmitz et al., 2018). PEST mutations identify genetic subtypes of B cell lymphoma with a worse prognosis (Arruga et al., 2014; Baliakas et al., 2015; Inamdar et al., 2016; Schmitz et al., 2018), suggesting the need to extend targeting Notch1 in these aggressive forms of B cell malignancies.

The Notch signaling pathway is also frequently activated in multiple types of solid tumors (Lobry et al., 2011; Stransky et al., 2011), such as melanoma, colorectal carcinoma, and cholangiocarcinoma through mechanisms that differ from genetic variations (Roy et al., 2007; Wang et al., 2014). Paradoxically, mutations that inactivate the Notch pathway have been described in several human cancers as well (Klinakis et al., 2011; Stransky et al., 2011), showing that, depending on the cellular context, Notch signaling can be oncogenic or tumor suppressive, and suggesting that fine-tuned inhibition of Notch signaling could be useful in those situations where Notch is activated.

The preponderance of oncogenic *NOTCH1* mutations in lymphoid malignancies has prompted the search for effective anti-Notch1 therapeutics (Baldoni et al., 2018; Roti and Stegmaier, 2011, 2014). Because Notch activation relies on γ-secretase-mediated proteolysis, γ-secretase inhibitors (GSIs) had entered in clinical trials to treat relapsed T-ALL. However, the first generations of GSIs were poorly tolerated because of on-target gastrointestinal toxicity (DeAngelo et al., 2006; Golde et al., 2013; van Es et al., 2005). As shown by Riccio et al. (2008), the toxic effect of GSIs are a consequence of lack of substrate specificity of these molecules resulting in the combined inhibition of wild-type NOTCH1 and NOTCH2 in intestinal progenitor cells. Although few patients achieved a complete response, GSIs exhibited moderate clinical activity in some patients with solid tumors and leukemia (Knoechel et al., 2015). Recently, several studies demonstrated that combining GSIs with chemotherapy or other targeted agents increases the anti-cancer effects of these drugs (Groeneweg et al., 2014; Mukherjee et al., 2016; Schott et al., 2013; Yuan et al., 2015), supporting the development of innovative anti-NOTCH1 therapeutics.

We have previously established that a small-molecule inhibitor of SERCA (sarco/endoplasmic reticulum calcium ATPase), thapsigargin, inhibits NOTCH1 and possesses anti-leukemia activity in a mouse model of human T-ALL. Importantly, thapsigargin preferentially inhibits the maturation of mutant NOTCH1 receptors compared with wild-type NOTCH1 and NOTCH2 receptors. This selectivity provides a therapeutic window not observed before with other Notch modulators, including GSIs or antibody-based approaches (Roti et al., 2013; Sorrentino et al., 2019). However, thapsigargin binding to SERCA results in an increase in cytosolic Ca^{2+} concentration and a depletion of Ca^{2+} stored in the endoplasmic reticulum (ER). Thus, the delivery of free thapsigargin to humans might cause cardiac toxicity due to a calcium ion shift. To overcome this limitation, we generated a thapsigargin pro-drug to deliver the small molecule in T-ALL. To this end, we took advantage of the dependency of ALL on folic acid and tagged folate to a permissive site on an active alcohol derivative of thapsigargin (8-O-debutanoylthapsigargin) via a cleavable ester linkage (JQ-FT) (Roti et al., 2017). However, an alternative approach to reduce the potential toxicity of thapsigargin is through the identification of SERCA inhibitors that retain the anti-Notch properties but lack Ca^{2+}-related toxicities.

In this work, from a series of P-type ATPase inhibitors we optimized and characterized the effect of the selective SERCA modulator CAD204520 in *NOTCH1*-mutated T-ALL. We demonstrate that CAD204520 exhibits a reduced Ca^{2+}-related toxicity but retains anti-Notch1 and anti-leukemia capacity both *in vitro* and *in vivo* in *NOTCH1*-mutated T-ALL models. Furthermore, by extending the testing of CAD204520 in B cell malignancies carrying clinically relevant PEST mutations, we demonstrate the potential of SERCA inhibition as a therapeutic approach against these cancers.

RESULTS

Identification of CAD204520 as a Selective Ca^{2+} ATPase Inhibitor

P-type ATPases are a group of evolutionarily conserved proteins that transport a variety of charged substrates, such as H^+, Na^+, K^+, Ca^{2+}, Zn^{2+}, and Cu^+ or phospholipids across membranes (Bublitz et al., 2011). Because P-type ATPases control active ion transport across cellular membranes, their altered activity is associated with the development of pathophysiological conditions, including cardiovascular, neurological, renal, and metabolic diseases. Consequently, P-type ATPases are compelling therapeutic targets. For example, the cardiac Na^+/K^+-ATPase inhibitor, digoxin (Hauptman and Kelly, 1999), and gastric H^+, K^+-ATPase inhibitor, omeprazole (Sachs, 1997), are among the most clinically successful therapeutics in this target class (Burghoorn et al., 2002).

In recent years, P-type ATPases (e.g., SERCA) have emerged as potential dependencies in cancer (Yatime et al., 2009) and as mediators of chemotherapy resistance in solid tumors (Li et al., 2012; Samimi et al., 2004). Their importance for cell survival has furthermore sparked an interest in inhibiting P-type ATPases of pathogenic fungi and bacteria (Seto-Young et al., 1997). To identify potent P-type ATPase inhibitors in this context, Kjellerup et al. (2017) screened a library containing nearly 191,000 compounds for inhibition of the fungal H^+-ATPase. A total of 407 compounds inhibited ATP hydrolysis activity of the H^+-ATPase by greater than 50% and were subsequently counter-screened for P-type ATPase specificity, by testing their effect on mammalian SERCA (rabbit SERCA1a, which shares 96.6% protein similarity with human SERCA orthologs) and pig Na^+/K^+-ATPase (Bublitz et al., 2018; Clausen et al., 2017; Kjellerup et al., 2017) (Figure 1A).

The initial hit compound, 2-(2-pyridyl)-6-(trifluoromethoxy)-1H-indole (Figures 1BI, and S1A), was a weak inhibitor of SERCA ATPase (half maximal inhibitory concentration [IC_{50}] = 236 μM) but with an attractive low molecular weight. An extensive exploration of the chemical space occupied by the pyridine core was

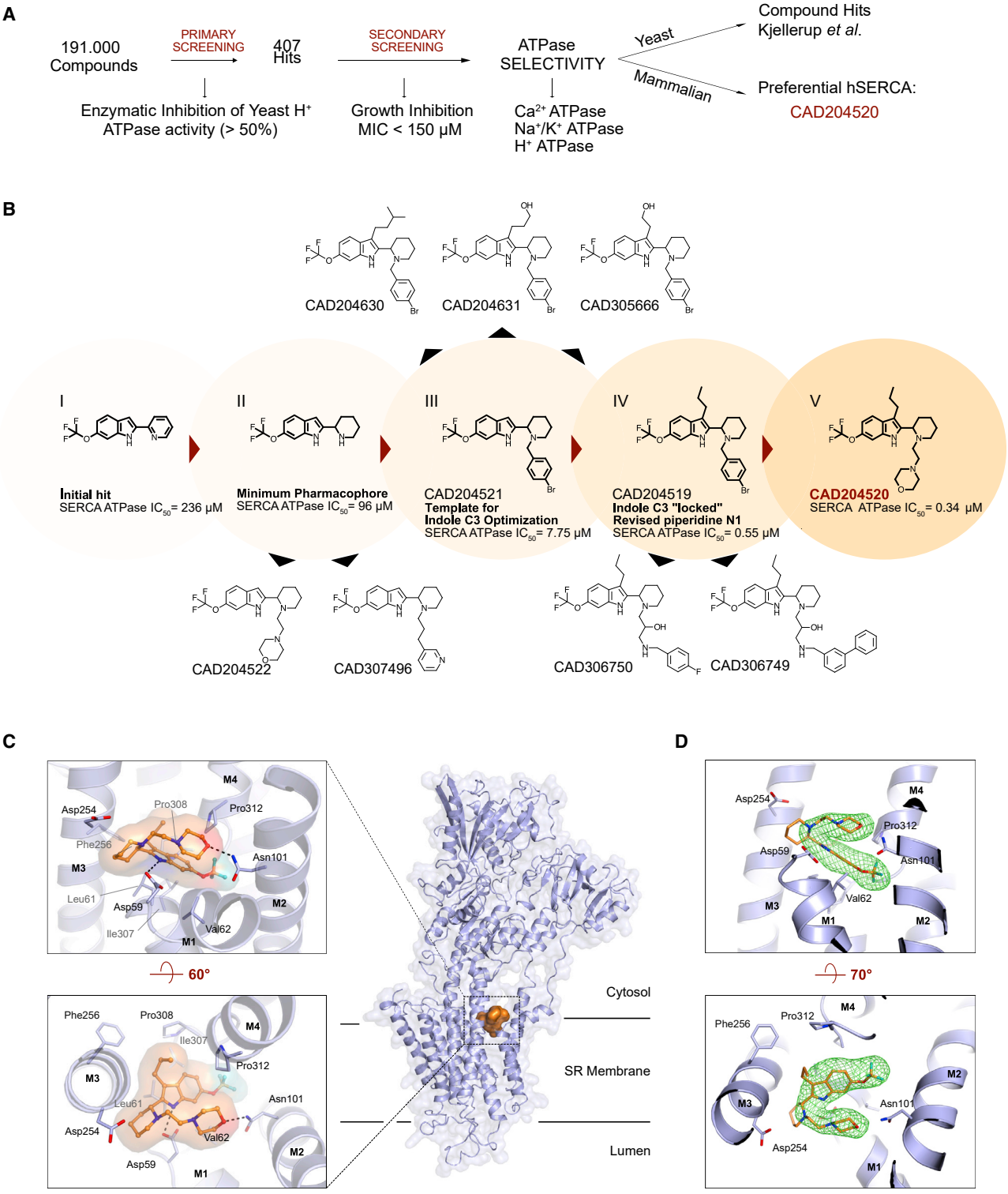

Figure 1. Identification, Structure-Activity Relationship and Co-crystal Structure of CAD204520

(A) Identification of CAD204520. A total of 191,000 small molecules were screened for inhibition of the fungal H^+-ATPase Pma1. Molecules with an enzymatic inhibition of the H^+-ATPase that exceed 50% were retained for subsequent hit validation. The 407 molecules were counter screened for (Pma1 over SERCA or Na^+/K^+) ATPase selectivity and minimum growth inhibitory capacity (MIC) <150 µM. Hits were then characterized as described in Kjellerup et al. (2017). From a subsequent hit optimization program (see B), CAD204520 was identified as the most promising candidate against mammalian Ca^{2+}-ATPase (SERCA).

(B) Structure-activity relationship (SAR) of CAD204520.

(legend continued on next page)

performed through a systematic replacement with commercially available alternative heteroaromatic and heterocyclic systems, as well as pyridines substituted with small functional groups capable of picking up polar interactions. As a result, the piperidine analog 2-(2-piperidyl)-6-(trifluoromethoxy)-1H-indole (Figure 1BII) was identified as the minimum pharmacophore with improved SERCA ATPase potency, selectivity against Na^+/K^+-ATPase, and a reasonable ligand efficiency of 0.28. Options for diversity in substitution of indole C4-C7 were limited and C6-OCF_3 was "locked" to continue exploration of more promising points of substitution. Furthermore, indole N1 had been extensively explored in a closely related chemical program with an overlapping pharmacophore, and for reasons of concern about target selectivity it was decided not to explore the indole N1 chemical space with the identified compound II. Conversely, compound II was explored in R^1 of the indole system and R^2 of the piperidine system (Figure S1B) for reasons detailed below.

Compounds with substitution on piperidine N1 (R^2) with R^1 = H were subsequently produced and, among them, CAD204522, CAD307496, and CAD204521 (Figure 1B) showed various degrees of Ca^{2+}-ATPase activity (Table S1). Interestingly, CAD204521 (Figure 1BIII; Table S1) was closely related to a previously reported potent fungal H^+-ATPase inhibitor, Compound 7 (Bublitz et al., 2018). Similarly to Compound 7, CAD204521 showed an improved potency against Ca^{2+} ATPase but not a desired selectivity or drugability profile. Because indole C3 had the potential to provide Ca^{2+}-ATPase selectivity, we decided to explore indole R^1 with R^2 = p-bromobenzyl (derivatives of CAD204521, Figure 1BIV). For example, CAD204519 was by far the most potent inhibitor of Ca^{2+}-ATPase; however, with an unfavorable Na^+/K^+ Ca^{2+} selectivity. Nevertheless, substitutions with certain hydrophilic groups on the R^2 on piperidine N1 (Figure 1B; Table S1, CAD306750, CAD306749, and CAD204520) increased the selectivity toward mammalian SERCA.

Notably, CAD204520 (Figure 1BV and S1C) preferentially inhibited the Ca^{2+}-ATPase by reducing its ATP hydrolysis activity with an IC_{50} of 0.34 ± 0.03 μM as compared with Na^+/K^+-ATPase (IC_{50} = 8.30 ± 0.94 μM) and H^+-ATPase (IC_{50} = 26.90 ± 2.98 μM) (Figure S1D; Table S1). Furthermore, CAD204520 displayed the overall most promising drug properties of the synthesized compounds with a calculated LogP of 4.4 and $LogD_{7.4}$ of 2.2 (ACD/Labs 18.1.1). This compound was thus selected for further studies as a selective SERCA inhibitor.

To assess the binding mode of CAD204520 to SERCA, we then crystallized it in complex with SERCA and determined the crystal structure at 3.4 Å resolution. The crystals were of the same space group as previously reported thapsigargin-bound SERCA (PDB: 2AGV), and the overall conformation of SERCA bound to CAD204520 is very similar to the thapsigargin-bound form. The CAD204520 ligand binds to a groove at the membrane interface of SERCA, between transmembrane helices M1, M2, M3, and M4 (Figures 1C and 1D), with two polar interactions to Asp59 on M1 (2.9 Å) and Asn101 on M2 (2.7 Å), and with several hydrophobic interactions involving Leu61, Val62, Ile307, Pro308, and Pro312 (Figure 1C). Interestingly, the CAD204520 binding groove is different from that of thapsigargin (Figure S1E), but similar to the binding of other SERCA inhibitors, such as cyclopiazonic acid (CPA) (Laursen et al., 2009) (Figure S1F) and 2,5-di-t-butyl-1,4-benzohydroquinone (BHQ) (Obara et al., 2005) (Figure S1G), and to that of the Compound 7 previously reported by Bublitz et al. (2018) (Figure S1H). In fact, the indole system (core structure) of CAD204520 superposes very closely on the tetrahydrocarbazole core of Compound 7, including the central interaction of the indole N1 nitrogen with Asp59. The morpholinoethyl group, interacting with Asn101, occupies the same space as one of the two alternative positions found for the bromophenyl moiety of Compound 7 (Figure S1H). In contrast to Compound 7, however, there is no interaction with Asp245. Despite this similarity, CAD204520 does not induce the same overall SERCA conformation as Compound 7, but a conformation almost identical to thapsigargin-inhibited SERCA. The thapsigargin-binding site lies adjacent to the CAD204520 site, separated by M3 (Figure S1I).

Collectively, these data show that CAD204520 selectively binds SERCA in the same binding pocket as BHQ, CPA, and Compound 7. This pocket has been identified as the pathway for Ca^{2+} ion entry into the pump from the cytosolic side of the membrane (Winther et al., 2013), and compound binding at this site locks SERCA in a Ca^{2+}-free (so-called *E2*) conformation.

CAD204520 Rescues T-ALL Cells from Thapsigargin Resistance

SERCA can be inhibited by different small molecules, such as thapsigargin, BHQ, 1,3-dibromo-2,4,6-tris (methyl-isothio-uronium) benzene, and CPA. These compounds have specific binding sites in the ATPase protein and hence different inhibitory mechanisms (Christensen et al., 1993). A first question is whether CAD204520 binding to SERCA mimics thapsigargin ATPase inhibitory kinetics or, rather, the two molecules act independently as predicted by structural data.

To test our hypothesis, we took two different approaches. First, we generated a T-ALL cell line (ALL/SIL) resistant to thapsigargin by selecting cells growing under increasing concentration of this molecule. At approximately days 90, 120, and 150, T-ALL cells displayed 2-, 10-, and 27-fold increased IC_{50} values, respectively (Figure S2A). To rule out that this drug resistance was mediated by altered expression of the target, we demonstrated that naive and resistant cell lines showed similar levels of SERCA2 and SERCA3 proteins (Figure S2B). To evaluate for thapsigargin-induced gene mutations within the *ATP2A 1–3* genes, we performed whole-exome sequencing and limited our analysis to single-nucleotide exonic missense variation

(C) Crystal structure of the SERCA-CAD204520 complex. Right panel: cartoon and surface representation of SERCA (light blue) with CAD204520 bound at the membrane interface (orange surface representation). Left panels: close-up of the CAD204520 binding sites, as seen parallel to the membrane (upper panel) or along the membrane normal (lower panel). Dashed lines indicate polar interactions with Asp59 (2.9 Å) and Asn101 (2.7 Å). Nitrogen is shown in blue, oxygen in red, and fluorine in cyan. Carbon is light blue for SERCA and orange for CAD204520.

(D) Simulated annealing omit map (green mesh) of CAD204520 (orange), contoured at 3.0 sigma. Top panel, viewed roughly along the membrane plane; bottom panel, viewed roughly perpendicular to the membrane.

See also Figure S1 and Table S1.

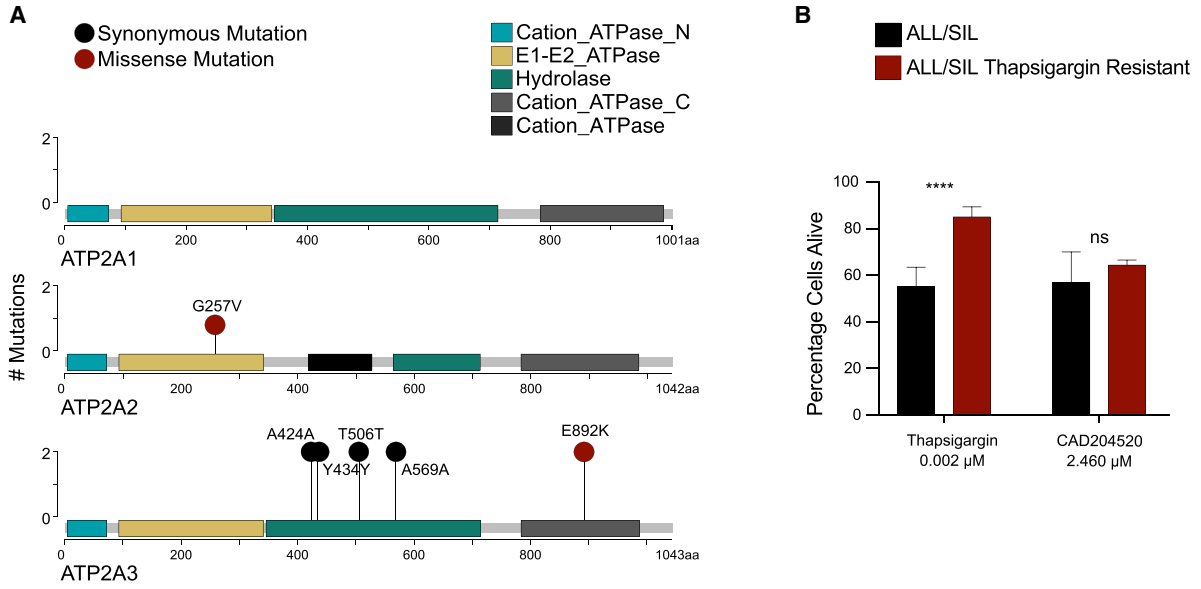

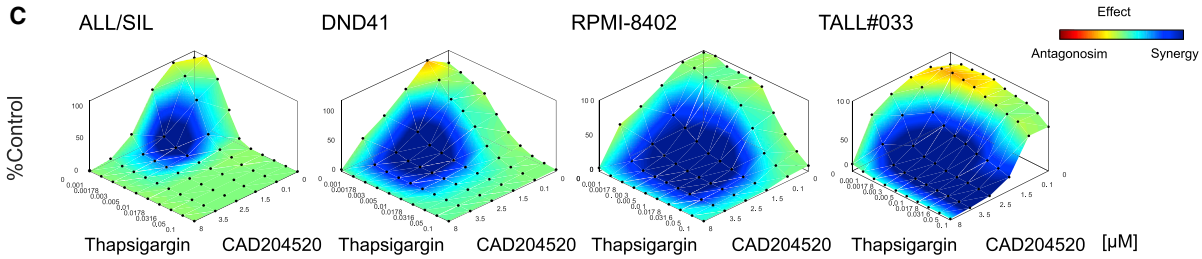

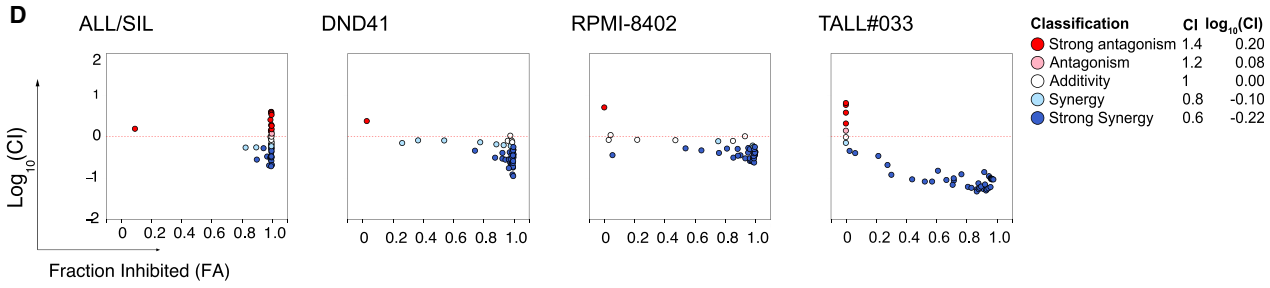

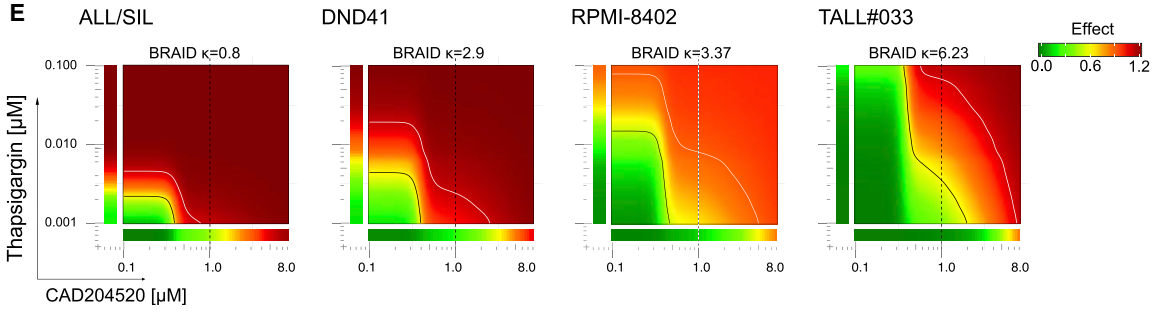

(legend on next page)

with a Phred-scaled quality score >30 (standard error = 1/1,000 = 0.1%; accuracy 99.9%) (Figure S2C). Previous work had demonstrated that mutations occurring in the third stalk (M3) segment of SERCA determine the sensitivity of ATPase to thapsigargin (Yu et al., 1998, 1999; Zhong and Inesi, 1998). In particular, mutations in the M3 segment between Asp^{254} and Leu^{260} increase the thapsigargin concentrations required for inhibiting SERCA by more than three orders of magnitude (Horn et al., 2018; Zhong and Inesi, 1998) (Figure S2D). Interestingly, in ALL/SIL-resistant cells we identified, within the Asp^{254}-Leu^{260} hotspot, a missense single-nucleotide polymorphism occurring in *ATP2A2* exon 8 (c.G770T) caused a $glycine^{257} \rightarrow$ valine mutation in the M3 helix (Figures 2A and S1I highlighted in red). No mutations occurred in *ATP2A1* (Figure 2A, top panel), while missense mutations in *ATP2A3* were present both in the naive and resistant lines, indicating a pre-existing mechanism of allelic variance (Figure 2A, bottom panel). Similarly, no acquired mutations were identified in *SEC24A*, a gene involved in ER-Golgi protein trafficking and previously identified as an essential mediator of thapsigargin-induced cell death in a genome-wide CRISPR/Cas9 screen in HAP1 cancer cells (Chidawanyika et al., 2018). According to our crystal structure, Gly^{257} faces a hydrophobic part of CAD204520 at a distance that could probably accommodate a valine residue without interfering with CAD204520 binding (Figure S1I). The introduction of the bulky valine side chain will, however, very likely limit the freedom of movement of the neighboring residue Phe^{256}, which has to swing sideways to accommodate thapsigargin binding (Figures S1E and S1I), thus providing a potential explanation for the resistance effect.

Next, we treated ALL/SIL naive and resistant cells at ALL/SIL IC_{50} (as shown in the following sections) concentrations, and demonstrated that $G^{257} \rightarrow V$ rescues ALL/SIL cells from thapsigargin-induced cytotoxicity while it does not interfere with CAD204520 effects (Figure 2B). Accordingly, because CAD204520 binds to SERCA in a pocket similar to that of CPA but distinct to that of thapsigargin, we anticipated that the combined inhibition might result in a synergistic effect with thapsigargin but not with cyclopiazonic acid. To avoid the limitations and biases associated with any one algorithm used to study drug-drug interactions, we used comprehensive approaches, including the Loewe additivity model, the Chou and Talalay index, and the Bivariate Response to Additive Interacting Doses (BRAID) analysis. The Loewe additivity is a commonly used dose-effect-based model to quantify a zero-interactive state for the combination of two drugs (Loewe, 1953). The Chou-Talalay method (Chou, 2010) for drug combination is based on the median-effect equation and provides a mechanism-independent method for quantitative determination, combination index (CI), of drug interactions. A CI ranging from 0.9 to 1.1 is considered additive, a CI < 0.9 indicates synergy, and a CI > 1.1 resistance. Finally, we used a response surface method, the BRAID model of combined action (Twarog et al., 2016, 2018). A κ BRAID index > 0 shows synergy between the compounds tested. Unlike most methods that reduce combination analysis to a simple decision between synergy, additivity, and antagonism, surface models use non-linear optimization to fit a response surface model to the effects of combined compounds. We tested CAD204520 and thapsigargin both individually and in combinations at the indicated concentrations for a total of 60 combinatorial points in T-ALL cell lines and in primary *NOTCH1*-mutated T-ALL samples. We found that simultaneous exposure to CAD204520 and thapsigargin for 72 h resulted in a robust synergistic inhibition of cell viability in T-ALL cells. Loewe, CI, and BRAID models established a synergistic effect at low-dose combinations and support the notion that CAD204520 binds at a site within SERCA that is distinct from the thapsigargin-binding sites (Figures 2C–2E). Consistent with our hypothesis, combined CAD204520 and CPA treatment did not demonstrate the same degree of synergistic activity (Figure S2E).

Collectively, these data indicate that G257V mutation in the M3 helix of SERCA do not interfere with CAD204520 activity and that a greater anti-leukemia effect may be achieved by the simultaneous binding of CAD204520 and thapsigargin to their respective sites in SERCA.

CAD204520 Suppresses Leukemia Growth in *NOTCH1*-Mutated T-ALL and MCL

We previously demonstrated that SERCA inhibitors decrease T-ALL growth both *in vitro* and *in vivo* (Roti et al., 2013). To validate CAD204520 as a potential modulator of Notch-dependent cancers we initially tested the effect of CAD204520 in a panel of T-ALL or MCL cell lines that contain activating mutations in the HD of *NOTCH1* and/or deletions in the degradation domain (PEST) (Figure S3A). *NOTCH1*-mutated T-ALL (Figure 3A) (ALL/SIL, CTV-1, DND41, PF382, and RPMI-8402) or MCL cell lines

Figure 2. CAD204520 Overcomes Thapsigargin Resistance in T-ALL

(A) Lollipop graphs showing sequenced mutations in the exonic region of *ATP2A1*, *ATP2A2*, and *ATP2A3* genes. Allelic variants are depicted with a circle (black, synonymous; red, missense) relative to their amino acid position (gray bottom bar, aa) and to their protein domains (color coded). The length of the lollipop (number of mutations) bar indicates: if 0, no mutations occur; if 1, mutations occur in one sample; if 2, mutations occur in both samples.

(B) Effect of CAD204520 and thapsigargin and CAD204520 treatment in naive and resistant ALL/SIL cells lines. Histograms show percentage of cells alive after 72 h of treatment at the indicated concentrations (~IC_{50}). Error bar denotes the mean ± SD of a minimum of three replicates. Statistical significance among groups (****$p \leq 0.0001$) was determined by one-way ANOVA.

(C) Surface plots analysis of ALL/SIL, DND41, and RPMI-8402 T-ALL cell lines and a primary *NOTCH1*-mutated T-ALL sample treated with vehicle, CAD204520, thapsigargin, or CAD204520 plus thapsigargin. Each point represents an independent measurement representative of three biological replicates. Plots were generated using the Combenefit script by MATLAB R201, which represents the Loewe (dose-effect-based approach) analysis. A color scale bar represents the level of drug antagonism or synergism.

(D) Combination index analysis for the combinations of CAD204520 with thapsigargin in ALL/SIL, DND41 and RPMI-8402 T-ALL cell lines and a primary *NOTCH1*-mutated T-ALL treated for 3 days. On the y axis is represented the combination index, on the x axis the fraction of cells inhibited.

(E) BRAID index analysis for the combinations of CAD204520 with thapsigargin in ALL/SIL, DND41, and RPMI-8402 T-ALL cell lines and a primary NOTCH1-mutated T-ALL treated for 3 days. A color scale bar represents the level of drug antagonism or synergism. K index is indicated.

See also Figure S2.

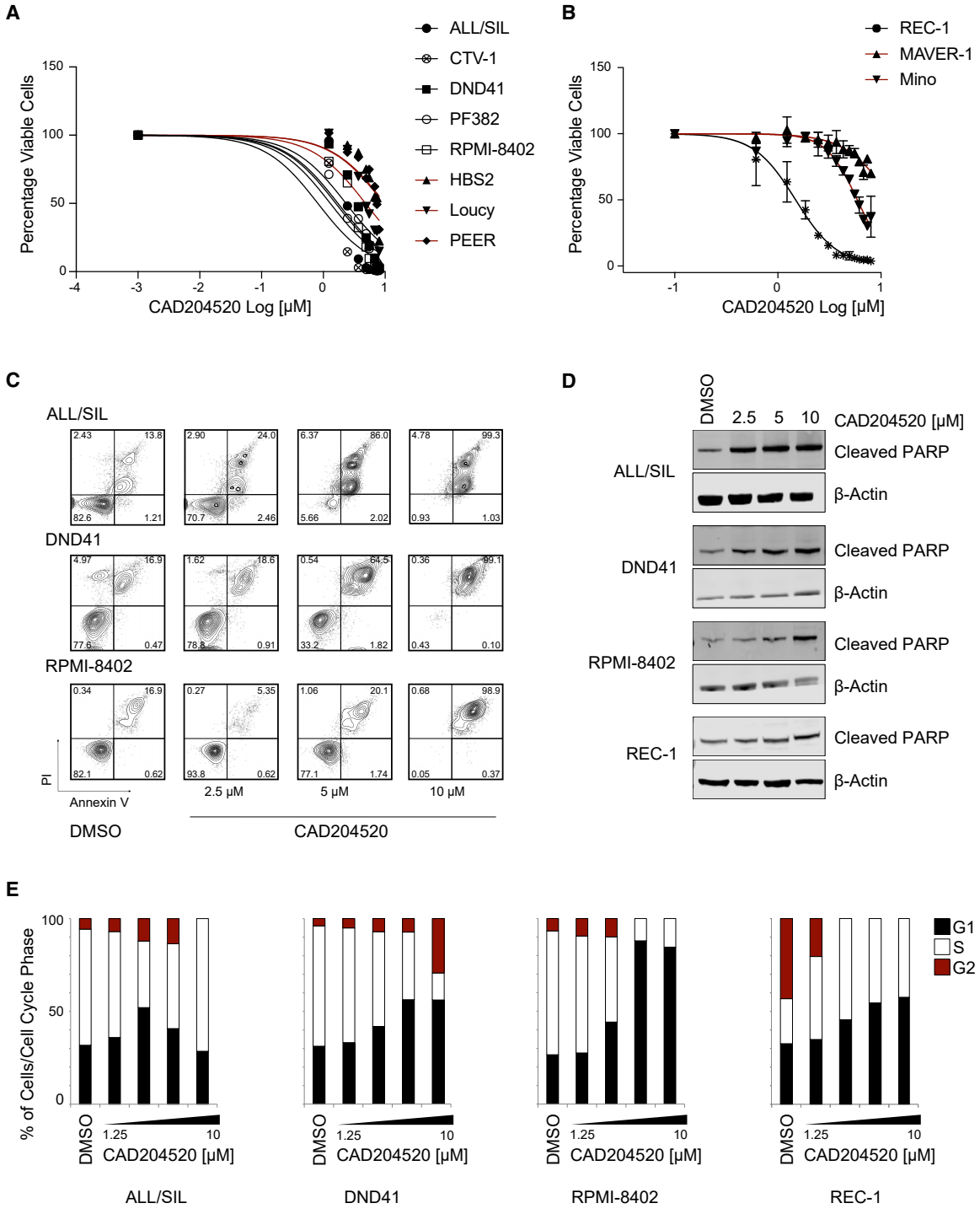

Figure 3. CAD204520 Impairs T-ALL Proliferation

(A) Effect of CAD204520 on cell viability after 72 h of treatments in the indicated T-ALL cell lines. Error bars denote ± SD of two replicates.

(B) Effect of CAD204520 on cell viability after 72 h of treatments in the indicated MCL cell lines. Error bars denote ± SD of two replicates.

(C) Effect of CAD204520 treatment on induction of apoptosis. Annexin V/propidium iodide staining of T-ALL cells after 72 h of treatment with the indicated concentrations of CAD204520. A minimum of 20,000 events was collected for each condition.

(D) Western immunoblot showing expression of cleaved PARP in *NOTCH1*-mutated cell lines (ALL/SIL, DND41, RPMI-8402, and REC-1) cells treated at the indicated concentrations of CAD204520 for 24 h. β-Actin was used as a loading control.

(E) Effect of CAD204520 treatments on cycling ALL/SIL, DND41, RPMI-8402, and REC-1 cells. Percentage of DNA content after 4 days of treatment with the indicated concentrations of CAD204520 on each cell-cycle phase is indicated. A minimum of 20,000 events was collected for each condition.

See also Figure S3.

(legend continued on next page)

suppressed by GSI (REC-1) (Figure 3B) (Weng et al., 2004) were more sensitive to CAD204520 as measured by inhibition of cell viability compared with *NOTCH1* wild-type tumor cells (Figures S3B and S3C). Seventy-two hours of CAD204520 treatment triggered concentration-dependent apoptosis as determined by the increase of Annexin V/PI$^+$ cells (Figure 3C) and the cleavage of PARP proteins (Figure 3D).

An additional phenotypic consequence of NOTCH1 inhibition with GSI is that T-ALL cells undergo cell-cycle arrest (Weng et al., 2004). As shown in Figure 3E, CAD204520 induced a G0/G1 arrest preferentially in *NOTCH1*-mutated tumors (Figure S3D), and together with the data described above it supports the notion that CAD204520 inhibits lymphoid-derived cancer cells carrying clinically relevant *NOTCH1* HD or PEST mutations.

CAD204520 Suppresses Notch1 Signaling

NOTCH receptors undergo several processing events, including a first cleavage by a furin-like convertase (S1) in the *trans*-Golgi network that generates full-length heterodimers (Blaumueller et al., 1997; Logeat et al., 1998) ready to be conveyed to the plasma membrane (Le Borgne, 2006). The correct folding of these heterodimers requires Ca^{2+} that, in physiological condition, is tightly regulated across the ER storage by SERCA (Chemaly et al., 2018).

To support the hypothesis that CAD204520-mediated SERCA inhibition impairs mutant NOTCH1 maturation, we evaluated the expression of NOTCH1 full-length and transmembrane portions of CAD204520-treated cells by western blotting. Lysates from T-ALL cell lines treated with 5 μM CAD204520 for 24 h were immunoblotted with an antibody specific for the cytoplasmic portion of NOTCH1 that recognizes both unprocessed NOTCH1 (FL-N1) (~270 kDa) and the furin-processed transmembrane subunit (TM-N1) (~110 kDa). CAD204520 reduced the levels of the furin-processed transmembrane NOTCH1 subunit, but not the unprocessed full-length NOTCH1 precursor, in multiple T-ALL cell lines (Figure 4A). As expected from our structural data, combined CAD204520 and thapsigargin treatment resulted in an enhanced reduction in ICN1 and TM-NOTCH1 levels (Figure S4A).

In addition, we demonstrated that treatment of T-ALL with CAD204520 resulted in a concentration-dependent decrease in NOTCH1 expression on the cell surface by flow cytometry (Figure 4B). As expected, we did not observe this effect with a known GSI Notch inhibitor N-[N-(3,5-difluorophenacetyl)-1-alanyl]-(S)-phenylglycine. Consistent with our hypothesis that CAD204520 affects NOTCH1 maturation rather than expression, NOTCH1 only decreases at the surface of the cells upon CAD204520 treatment, but co-localizes at the ER-Golgi intermediate compartment as shown by immunofluorescence co-localization studies (Figures 4C and S4B–S4E). An immediate consequence of the decrement in NOTCH1 on the surface of the cells is the reduction of the catalytic activity of the γ-secretase complex because of the lack of NOTCH1 substrate. Here, we would expect a reduction in the level of ICN1. Indeed, CAD204520 ultimately leads to loss of ICN1 (Figure 4D) and results in the suppression of NOTCH1 target genes *MYC* and *DTX1* as measured by RT-PCR (Figure 4E). Furthermore, testing CAD204520 in MCL *NOTCH1*-mutated cells yielded results comparable with the one described in T-ALL, suggesting a conserved mechanism across different *NOTCH1*-mutated cancers (Figure S4D-F).

In summary, these data show that CAD204520 inhibits Notch1 maturation, demonstrating that SERCA inhibitors with a binding mode different from thapsigargin can efficiently suppress NOTCH1 maturation.

CAD204520 Preferentially Inhibits NOTCH1-Mutated Cancers

SERCA inhibitors increase the Notch therapeutic index by targeting clinically relevant *NOTCH1* mutations in leukemia cells (Roti et al., 2013, 2017; Sharma et al., 2015). In fact, leukemia cells carrying *NOTCH1* alleles with HD mutations are more sensitive to SERCA inhibition than cells with wild-type *NOTCH1* alleles (Roti et al., 2013, 2017).

To verify the hypothesis that CAD204520 preferentially targets mutant NOTCH1, we used two T-ALL cell lines carrying the same t(8; 14) (q24; q32)/*TRAD@-MYC* translocation but different Notch mutational status (Figures 5A and S5A). SKW-3/KE-37 harbors an isolated *NOTCH1* mutation in the PEST domain, while MOLT16 is *NOTCH1* wild type (Minowada et al., 1989; Weng et al., 2004). First, we determined that the mutant T-ALL cell line was more sensitive to CAD204520 growth inhibition as measured by an ATP-based cell viability assay (Figure S5B). To validate this observation, we established a flow cytometry-based competition assay. SKW-3/KE-37 were transduced with a GFP lentiviral expressing vector and co-cultured with MOLT16 T-ALL cells in a 1:1 ratio. Next, we treated SKW-3/KE-37-GFP and MOLT16 co-cultured cells with increasing concentrations of CAD204520 and demonstrated that the mutated T-ALL cell line, SKW-3/KE-37-GFP, was more sensitive to growth suppression compared with wild-type MOLT16, as quantified by flow cytometric analysis of alive versus dead cells (Figure 5B). Analysis of caspase-3 and -7 activities indicates that the *NOTCH1* mutational status sensitizes cells to CAD204520-mediated apoptotic cell death (Figure 5C). Consistent with the hypothesis that SKW-3/KE-37 relies on Notch signaling for growth and survival, we observed a decrement of NOTCH1 protein only in mutant T-ALL cells compared with wild-type cells (Figure 5D).

To further support the preclinical development of CAD204520, we tested it (dose range = 0.6–8 μM) in a collection of T cell lymphoblasts isolated from T-ALL patients. As shown in Figure 5E, CAD204520 preferentially affects T-ALL viability compared with normal lymphocytes. Primary blasts, derived from a patient suffering from a *NOTCH1*-mutated T-ALL, exposed to 5 μM CAD204520, rapidly underwent apoptosis (Figure S5C). In addition, T-ALL primary cases for which we confirmed a *NOTCH1* mutation (no. 1 *NOTCH1* ex 27, c.5101G > C p.A1701P; no. 2 *NOTCH1* ex 26, c.4793G > C p.1598P and *FBXW7* ex 9, c.1514G > T p.R505L) were more sensitive to CAD204520 compared with *NOTCH1* wild-type B cell ALL (Figure 5F).

Collectively, these results indicate that CAD204520 retains anti-tumor activity preferentially in cells carrying *NOTCH1* alleles with HD or PEST mutations, holding great promise for CAD204520 future development against this indication.

Consequences of Ca^{2+} Release upon CAD204520 Treatment

A consequence of SERCA inhibition is the rise of intracellular Ca^{2+} followed by the depletion of Ca^{2+} stored in the ER. ER Ca^{2+} exhaustion triggers a number of secondary events,

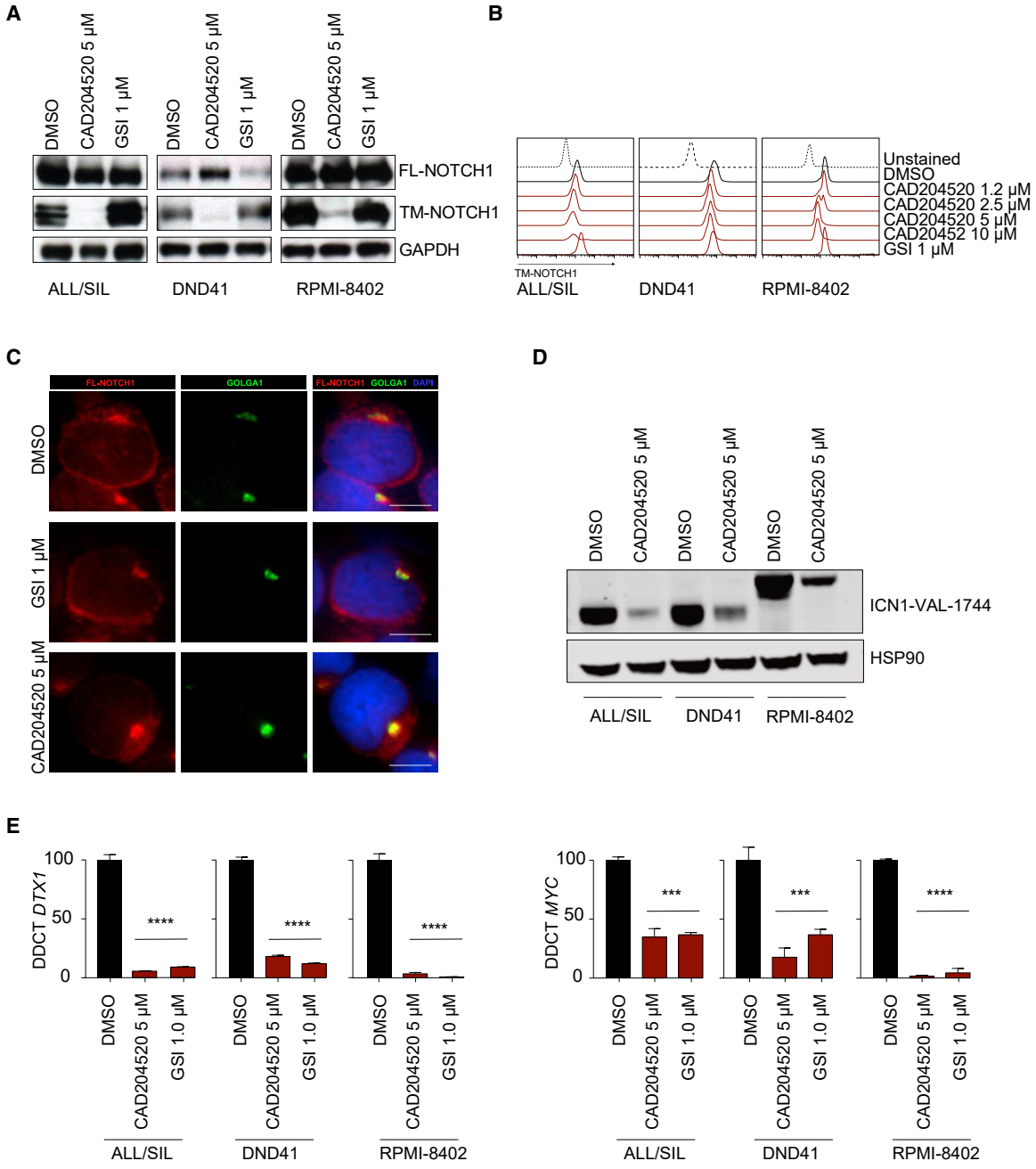

Figure 4. CAD204520 Modulates Notch1 Signaling

(A) Effect of CAD204520 treatment for 24 h on NOTCH1 (N1) processing and activation in T-ALL cell lines all with heterodimerization mutations (ALL/SIL [L1575PΔPEST], DND41 [L1594PΔPEST] and RPMI-8402 [ins1584PVELMPPE]). The blot was incubated with an antibody against the C terminus of NOTCH1 that recognizes both the furin-processed NOTCH1 transmembrane subunit (TM) and the unprocessed NOTCH1 precursor (FL).

(B) Effect of 24 h of CAD204520 and GSI (N-[N-(3,5-difluorophenacetyl)-1-alanyl]-(S)-phenylglycine [DAPT]) treatments on NOTCH1 cell surface staining as assessed by flow cytometry.

(C) Effect of CAD204520 and GSI (DAPT) treatment (24 h) on the subcellular localization of NOTCH1. Immunofluorescence images of permeabilized ALL/SIL incubated with anti-Notch1 (C20-red) and anti-Golgin (green) are shown. Co-localization is indicated by yellow signal. Scale bar, 100 μm magnification.

(D) Western immunoblot showing the expression of cleaved NOTCH1 (ICN1) in ALL/SIL, DND41, and RPMI-8402 cells treated at the indicated concentrations of CAD204520 for 24 h. HSP90 was used as a loading control.

(E) CAD204520 treatment for 24 h downregulates expression of NOTCH1 target genes in ALL/SIL, DND41, and RPMI-8402 T-ALL cells as assessed by qRT-PCR. Error bars indicate the mean ± SD of four replicates. Data were analyzed using the ΔΔCT method and plotted as a percentage relative to the control gene *RPL13A*. Statistical significance (***$p \leq 0.001$, ****$p \leq 0.0001$) was determined by one-way ANOVA using Bonferroni's correction for multiple comparison testing. GSI (DAPT) was used as a positive control.

See also Figure S4.

(legend continued on next page)

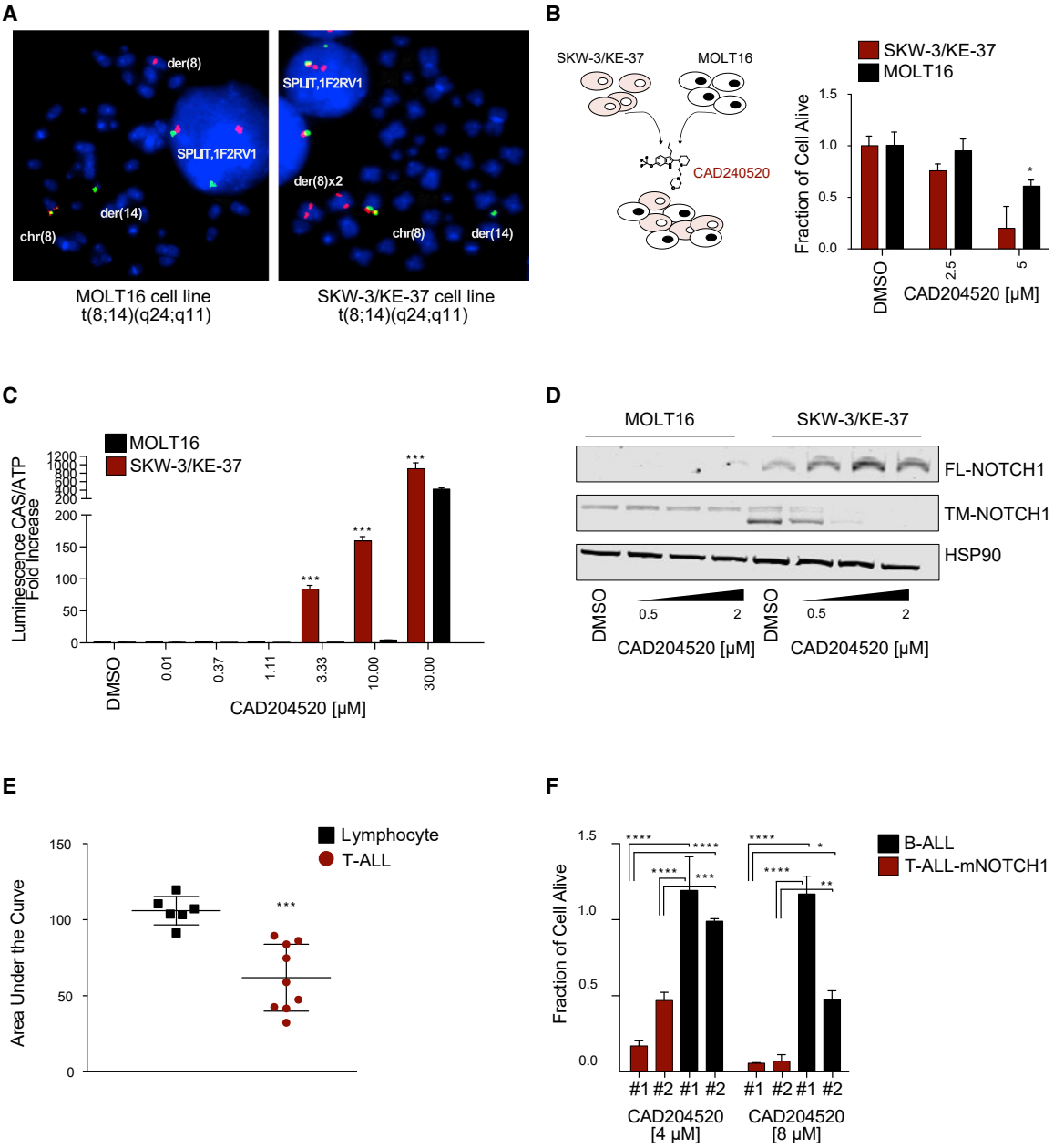

Figure 5. *NOTCH1* Mutation Sensitizes T-ALL Cells to CAD204520 Inhibition

(A) Interphase and metaphase FISH, with the LSI MYC probe, show split signals between der(8) (red signal) and der(14) (green signal), in the MOLT-16 (left) and SKW-3/KE-37 (right) cell lines. (b) SKW-3/KE-37 has two der(8).

(B) Left: cell-based competition assay. SKW-3/KE-37 and MOLT16 were transduced with a GFP-containing vector or an empty control vector, respectively, and co-cultured at a 1:1 ratio. Right: normalized effect of CAD204520 on cellular viability in co-cultured SKW-3/KE-37-GFP and MOLT16 cells treated for 72 h. Error bars denote the mean ± SD of two replicates for vehicle-treated (DMSO) cells and for CAD204520-treated cells. Statistical significance (*$p \leq 0.05$) was determined by one-way ANOVA using Bonferroni's correction for multiple comparison testing.

(C) Caspase-3/-7 luminescence fold induction in SKW-3/KE-37 and MOLT16 cells. Error bars denote the mean ± SD of six replicates for vehicle-treated (DMSO) cells and for CAD204520-treated cells. Statistical significance (***$p \leq 0.001$) was determined by one-way ANOVA using Bonferroni's correction for multiple comparison testing.

(D) Effect of CAD204520 treatment for 24 h on NOTCH1 (N1) processing and activation in SKW-3/KE-37 and MOLT16 cell lines. The immunoblot was stained with an antibody against the C terminus of NOTCH1 that recognizes the furin-processed NOTCH1 TM and the unprocessed NOTCH1 precursor (FL). HSP90 was used as a loading control.

(E) Effect of the CAD204520 in primary T-ALL cells (n = 9) or isolated lymphocytes (n = 6). The whisker plot represents the effect of small molecules on cellular viability calculated using the area under the curve (AUC) model of log-transformed dose-responses data using GraphPad v.7. The line in the whisker diagram

(legend continued on next page)

including the activation of the unfolded protein response (UPR) pathway (Wang and Kaufman, 2014), the activation of store-operated Ca^{2+} entry (Parekh and Putney, 2005), and ultimately cell death (Orrenius et al., 2003).

To quantify the consequences of CAD204520 or thapsigargin treatment at the level of cytosolic Ca^{2+}, we transferred ALL/SIL or DND41 in Ca^{2+}-free media and loaded with Indo-1 a ratiometric sensitive indicator fluorescent dye for measuring intracellular Ca^{2+}. As shown in Figure 6A compared with DMSO, CAD204520 slightly increases cytosolic Ca^{2+}. However, if compared with the thapsigargin effect, the extent of the increase appears modest with broad and flat peaks. In fact, thapsigargin causes a sharp rise in Ca^{2+} concentration at ~200 s upon drug injections. The next question is whether SERCA is still able to re-load Ca^{2+} from the cytosol inside the ER upon CAD204520 treatment. This hypothesis would explain why the increase of Ca^{2+} upon CAD204520 treatment is moderate and why thapsigargin triggers delayed on-target Ca^{2+} effects such as UPR activation and apoptosis (Lu et al., 2014). In this case we used a different approach and measured Ca^{2+} Fluo-3 AM epifluorescence using an IonOptix system. This approach is ideal to measure fluctuations of ER Ca^{2+}. As reported in Figure 6B, the peak fluorescence (f/f0_peak) was similar in the three groups of cells, indicating that the different compounds did not modify the Ca^{2+} release from the ER. Conversely, the fluorescence signal decay was significantly prolonged in thapsigargin-treated cells in comparison with both CAD204520 and DMSO (time_50%-f/f0; $p < 0.05$). In accordance with this finding, the fluorescence computed at 3, 5, and 10 min from the peak time (f/f0_3 min, 5 min, and 10 min) or the area under the dose curve calculated within the same time frame (control versus CAD204520 Δmean = 0.4188; control versus thapsigargin Δmean = −2.658; CAD204520 versus thapsigargin Δmean = −3.077), was significantly higher only in the thapsigargin group ($p < 0.05$ and $p < 0.0001$, respectively), suggesting that CAD204520 did not delay the cytosolic Ca^{2+} reuptake.

As previously mentioned, in addition to the effects on Ca^{2+} dynamics, thapsigargin and thapsigargin analogs activate the ER-related stress pathway of the UPR (Sehgal et al., 2017). To compare the effects of CAD204520 and thapsigargin on UPR activation we treated ALL/SIL, DND41, and RPMI-8402 at concentrations causing a similar ICN1 decrement (Figures 6C and S6A). Interestingly, only thapsigargin sustained the expression of validated UPR markers, such as P-eIF2α and the ER chaperone BiP (Grp78) (Figures 6C and S6A) or the proteolytic cleavage of ATF6 and its re-location in the nucleus (Figures 6D and S6B).

Sustained Ca^{2+} increase and UPR activation is associated with caspase-mediated apoptosis and cell death in several tissues (Sovolyova et al., 2014), including cardiac cells (Liu and Dudley, 2015). For example, Ca^{2+} release from the ER can induce delayed after-depolarizations leading to cardiac arrhythmias. Similarly, UPR activation has been found to play a role in arrhythmogenesis during human heart failure by affecting cardiac ion channel expression (Dally et al., 2009). Thus, we hypothesized, based on our Ca^{2+} dynamics studies, that cardiac cells may be more tolerant to CAD204520 compared with thapsigargin treatment. To validate this hypothesis, we tested CAD204520 and thapsigargin in HL-1 cardiac cells and demonstrated that HL-1 are less sensitive to SERCA inhibition compared with a *NOTCH1*-mutated cancer cell line, confirming that SERCA represents a strong dependency in T-ALL (Figures 6E and S6C). However, only cells treated with thapsigargin at IC_{50} concentrations displayed activation of the UPR pathway (Figure 6F), suggesting that CAD204520 further improves the therapeutic index of SERCA inhibitors because of its mild effect on Ca^{2+} dynamics and ER/UPR activation.

Modeling Preclinical Toxicity and Efficacy of CAD204520 in a T-ALL Leukemia Model

Because altered ER Ca^{2+} levels lead to heart failure (Yano et al., 2005), we measured the extent to which CAD204520 alters the function of heart cells. First, we isolated cardiomyocytes from Wistar rats and the cells were either untreated or incubated with CAD204520 or thapsigargin. The average diastolic sarcomere length (expressed in μm) exhibited comparable values in all cell groups, independent of the treatment and the time of exposure to the inhibitors (Control, 1.74 ± 0.006; $CAD204520_{2h}$, 1.75 ± 0.008; $CAD204520_{4h}$, 1.74 ± 0.007; Control, 1.76 ± 0.004; $Thapsigargin_{200nM}$, 1.76 ± 0.005; $Thapsigargin_{500nM}$, 1.76 ± 0.009). Compared with control cells, cardiomyocytes incubated with 5 μM CAD204520 for 2 h ($CAD204520_{2h}$) showed a reduced contractile efficiency, as reflected by the decrease in the rate of shortening ($-dl/dt_{max}$; Figure 7A; −27%) and re-lengthening ($+dl/dt_{max}$; Figure 7B; −25%), coupled with a lower fraction of shortening (FS; (Figure 7C; −27%). A further slight decline (approximately an additional 10% decrease) in cell mechanical performance was observed after 4 h exposure (data not shown). In accordance with cell contractile properties, $CAD204520_{2h}$ cardiomyocytes exhibited a modest (16%) decrease in the amplitude of the Ca^{2+} transient (Figure S7A) associated with a prolongation (+19%) of the time required for cytosolic Ca^{2+} removal (Figure S7B (Tau)). Choosing a thapsigargin dose for these comparative studies has been difficult due to the paucity of the *in vivo* studies reported in the literature. The dose selected for thapsigargin (200 nM) is in the mid-range of doses used by our group and others that assessed consequences of thapsigargin both *in vitro* and *in vivo* in different cancer models (Abdullahi et al., 2017; Ma et al., 2016; Roti et al., 2013). Nevertheless, thapsigargin induced a greater negative effect in treated cardiomyocytes. In fact, the rate of contraction, re-lengthening and the fraction of shortening were reduced by 77%, 89%, and 66%, respectively, compared with the control group, suggesting that thapsigargin, at the tested concentrations, causes a marked impairment of cardiac cell mechanics (Figures

represents the AUC median. The upper edge (hinge) indicates the 75th percentile of the dataset, and the lower hinge the 25th percentile. The ends of the vertical line show the minimum and the maximum data values. Statistical significance (***$p \leq 0.001$) was determined by a non-parametric t test (Mann-Whitney).
(F) Normalized effect of the CAD204520 in primary *NOTCH1*-mutated T-ALL cells (n = 2) or primary B-ALL cells (n = 2) on cellular viability. Error bars denote the mean ± SD of four replicates. Statistical significance comparing each T-ALL versus B-ALL case to each dose (***$p \leq 0.001$, ****$p \leq 0.0001$) was determined by a non-parametric t test (Mann-Whitney).
See also Figure S5.

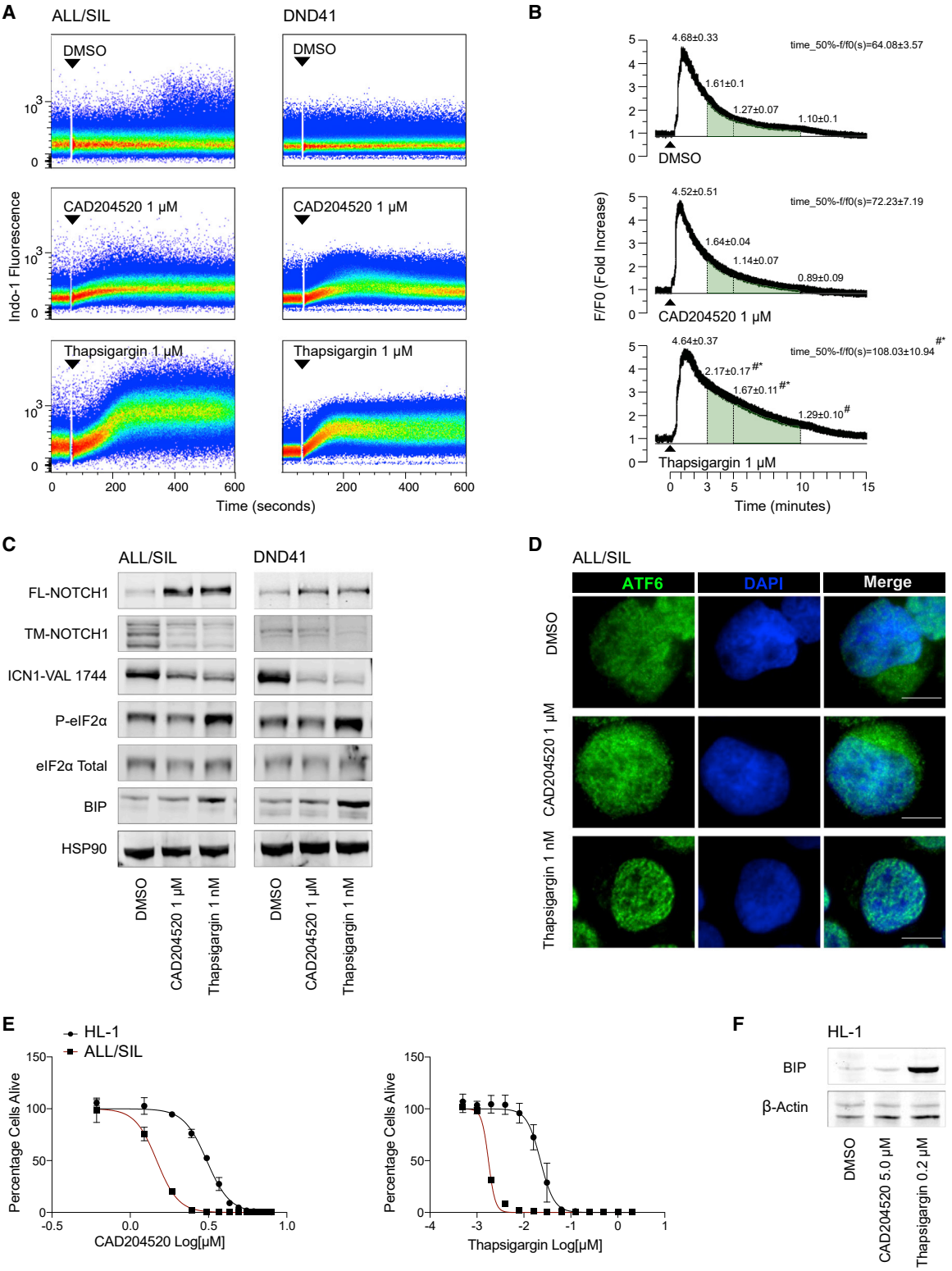

Figure 6. Effects of CAD204520 on Ca^{2+} and UPR Activation

(A) Indo-1 AM fluorescence traces of T-ALL cells loaded with 5 μM of Indo-1 AM and treated with DMSO, CAD204520 1 μM, or thapsigargin 1 μM. Baseline and post-treatment fluorescence is indicated by a black arrow. Cells were acquired for a minimum of 10 min on an LSR Fortessa X20 flow cytometer.

(legend continued on next page)

7A–7C). The thapsigargin-induced cell damage altered Ca^{2+} dynamics, as shown in the representative tracing reported in Figure S7C, hampering the measurement of Ca^{2+} transient parameters. Next, we evaluated the cytotoxic effect of CAD204520 on isolated cardiomyocytes by measuring the ability of the cells to produce ATP. Interestingly CAD204520 treatment only minimally affected the cellular metabolic capacity (10%) compared with vehicle-treated cells, suggesting that CAD204520 does not induce marked effects on cardiomyocyte viability at the times and conditions tested (Figure S7D).

We then assessed the translational significance of our results. To explore the utility of the CAD204520 as an *in vivo* chemical probe, we performed a bioavailability and tissue distribution study (pharmacokinetic study) of CAD204520 in CD1 mice and found the compound to have a T½ of 11 h, and C_{max} of 1.1 ng/mL (2.5 μM) at T_{max} = 1 h. Next, we completed a tolerability study in male and female BALB/c mice after administration of 30 mg/kg of CAD204520 BID by oral gavage for 21 days. Importantly, no adverse clinical symptoms or cardiac toxicity events were seen in animals dosed with vehicle or 30 mg/kg of CAD204520 (Figure 7D). Mice treated with double that dose (60 mg/kg) had mild reduction of weight (Figure S7E), without incurring cardiac failure, consistent with our *ex vivo* results. Animals were sacrificed at day 21. No gross pathological abnormalities were detected on visceral organs, including the heart, lungs, liver, brain, or kidney in treated animals. With this dosing schedule, we determined a C_{max} within the range of CAD204520 for biological activities as established *in vitro* (1–10 μM) and, therefore, initiated treatment studies of CAD204520 in a preclinical model of T-ALL.

To assess the *in vivo* efficacy of CAD204520, we established T-ALL-derived xenografts from SKW-3/KE-37 human T-ALL cell lines and confirmed leukemia engraftment by the quantification of $hCD45^{+}$cells in peripheral blood of transplanted mice (0.3% ± 0.2% circulating $hCD45^{+}$ cells 1 week before the start of treatment). Then, we treated our cohort at a dose of 45 mg/kg twice a day at 8 h intervals, for 4 days by oral gavage (Figure S7F). CAD204520 treatment resulted in a significant 56-fold reduction of the percentage of $hCD45^{+}$ SKW-3/KE-37 cells in circulating leukemic cells of xenotransplanted mice compared with the vehicle-administered control group (1.42% ± 2.6% versus 80.36% ± 4.5%; $p < 0.0001$) (Figures 7E and S7G) and, consistently, a reduction of leukemic infiltration in the spleen (Figures 7F and S7H). CAD204520-treated mice showed no decrease in body weight and no adverse effects on behavior. Importantly, no signs of acute cardiac toxicities (Figure 7G) or gastrointestinal metaplasia (Figure 7H) were documented. Furthermore, there were no changes in the complete blood counts between the control and treatment groups (Figure 7I).

Collectively these data demonstrate that CAD204520 reduces circulating leukemic cells without cardiac-related toxicity during short-term treatment in leukemia xenograft models, supporting further preclinical optimization in Notch1-dependent tumors.

DISCUSSION

Although the prognosis of T-ALL has improved over the last two decades, the outcome of T-ALL patients with primary resistant or relapsed disease remains poor (Litzow and Ferrando, 2015; Marks and Rowntree, 2017). Therefore, current research goals are focused on the identification of targets to develop more effective and less-toxic anti-leukemic agents (Follini et al., 2019; Roti and Stegmaier, 2011, 2014; Starza et al., 2019).

Several studies strongly support the development of Notch inhibitors for targeted therapy in hematological malignancies and solid tumors where Notch signaling is deregulated (Brzozowa-Zasada et al., 2017). For example, pan Notch pathway antagonism with GSISs reduces leukemia growth in mutant cancer cell lines and in mouse models (Palomero et al., 2006; Weng et al., 2004). Thus, modulators of Notch would be expected to have clinical efficacy particularly in T-ALL where recurrent *NOTCH1* mutations are common and cancer dependency has been well established. However, prolonged suppression of the canonical Notch pathway in normal tissue may cause dose-limiting gastrointestinal toxicity (DeAngelo et al., 2006) or increase the risk of skin cancers (Doody et al., 2015; Extance, 2010), underscoring the need for new therapeutic modalities to preferentially suppress the oncogenic signal. In recent years, we have pursued this approach and demonstrated that selective inhibitors of SERCA, such as thapsigargin and CPA, uniquely among Notch inhibitors, preferentially affect mutated NOTCH1 proteins compared with the wild-type ones (Roti et al., 2013, 2017).

Thapsigargin, a plant-derived sesquiterpene-γ-lactone, has been used extensively as a pharmacological tool to trigger Ca^{2+}-dependent and UPR pathways in several disease models (Lytton et al., 1991). Because the increase of cytosolic Ca^{2+} and sustained UPR activation (ER stress) are important mediators of apoptosis, SERCA inhibitors have been considered for cancer therapies (Mahalingam et al., 2013). However, large-scale isolation from *Thapsia* or scalable synthesis of thapsigargin

(B) Time course of ER calcium release and reuptake traces recorded in DMSO, CAD204520, and thapsigargin T-ALL-treated cells. Each trace is representative of five (DMSO) or four (CAD204520 and thapsigargin) independent experiments. In green the area under the curve (AUC). Values are reported as mean ± SEM; f/f0_peak, peak fluorescence normalized to baseline fluorescence; time_50%-f/f0, time at 50% of fluorescence signal decay measured from the peak time; f/f0_3min, 5min, and 10 min, fluorescence computed at 3, 5, and 10 min from the peak time. *$p < 0.05$ versus DMSO; #$p < 0.05$ versus 1 μM CAD204520. Statistical significance was determined by a Kruskal-Wallis test and differences among groups were determined by a Mann-Whitney non-parametric t test.

(C) Effect of CAD204520 and thapsigargin treatment for 24 h in ALL/SIL and DND41 cell lines. The blot was stained with an antibody against the C terminus of NOTCH1 that recognizes the furin-processed NOTCH1 TM and the unprocessed NOTCH1 precursor (FL), an antibody that recognizes the cleaved NOTCH1 (ICN1), P-eIF2α, total eIF2α, BiP, and HSP90 used as a loading control.

(D) Effect of CAD204520 and thapsigargin treatment for 24 h on ATF6 in ALL/SIL cell line. Immunofluorescence of permeabilized ALL/SIL cells stained with ATF6 (green) is shown. Cell nuclei were stained with DAPI (blue). Scale bar, 100 μm.

(E) Effects of CAD204520 (left) and thapsigargin (right) on cell viability after 72 h of treatments in HL-1 and ALL/SIL cell lines. Error bars denote ± SD of a minimum of two replicates.

(F) Effect of CAD204520 and thapsigargin treatment for 24 h in HL-1 cell lines. The blot was stained with BiP. β-Actin was used as a loading control.

See also Figure S6.

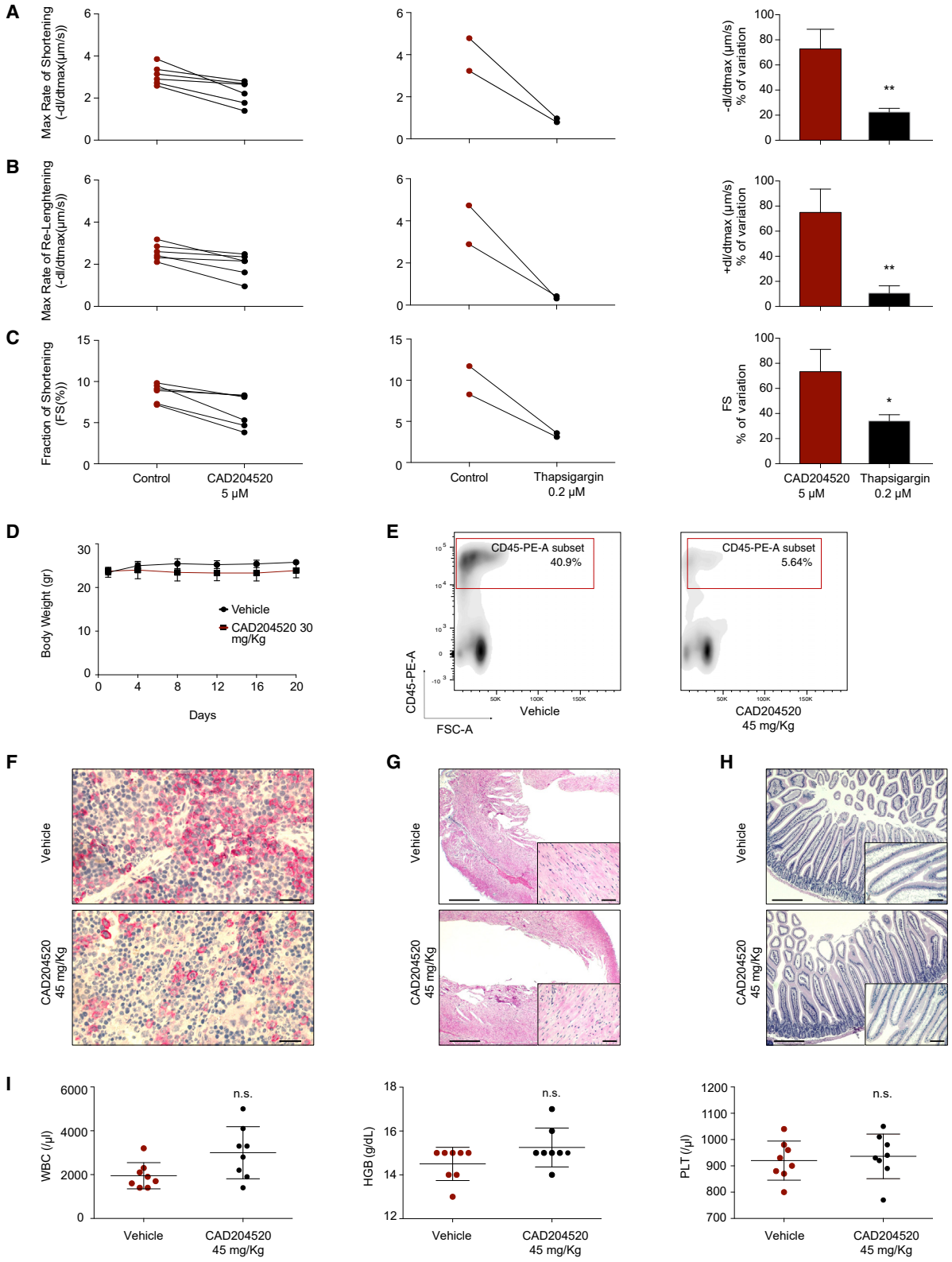

Figure 7. Effects of CAD204520 on Preclinical Model of T-ALL

(A–C) Left panels: effect of CAD204520 treatment on rat cardiomyocyte mechanics. Single experiments are represented by two dots interconnected by a solid line. Specifically, the line between the dots connects the quantification of maximal rate of shortening (A) ($-dl/dt_{max}$), maximal rate of re-lengthening (B) ($+dl/dt_{max}$),

(legend continued on next page)

is complex, requiring a 5- and 42-step process depending on the protocol used (Ball et al., 2007; Chen and Evans, 2017; Chu et al., 2017). Similarly, the synthesis of thapsigargin-based derivatives presents significant challenges. In fact, thapsigargin itself possesses a polyoxygenated 5-7-5 tricyclic core linked to four diverse ester groups and eight stereogenic centers not suitable for structural modeling (Ball et al., 2007; Ley et al., 2004). Structure-activity studies revealed that only few thapsigargin groups, for example, the ester bond at O(8), can be hydrolyzed to generate intermediate derivatives that can be used for conjugation with a peptide (Andersen et al., 2015; Mahalingam et al., 2016) or with a cleavable ester linkage (Roti et al., 2017). In addition, modification of the thapsigargin ester acyl group, or of the lactone carbonyl, significantly reduces thapsigargin activity in cells or biochemical assays, preventing their broad applicability in cancer (Quynh Doan and Christensen, 2015; Treiman et al., 1998).

A further limitation is that native thapsigargin is not tractable as a therapeutic agent due to expected Ca^{2+} shifts that can be prevented, for example, by creating inactive pro-drugs activated in a hysto-specific manner (Christensen et al., 2009; Doan et al., 2015). This is the mode of action of mipsagargin, a thapsigargin derivative currently undergoing clinical trials for solid tumors (Mahalingam et al., 2013). Our group has developed JQ-FT, a folate-thapsigargin derivative that leverages the dependency of leukemia cells on folate metabolism to direct the inhibitor into T-ALL cells (Roti et al., 2017). Another strategy is to exploit analogs that possess an enhanced selectivity toward SERCA isoforms preferentially expressed in cancer cells (Arbabian et al., 2011; Denmeade and Isaacs, 2005), while keeping the activity of SERCA2a, the major cardiac isoform, unaffected (Clark et al., 2010; Dally et al., 2010; Lipskaia et al., 2010).

An alternative is the development of small molecules that retain SERCA inhibitory capacities but have only transient effects on cytosolic Ca^{2+} shifts. This idea emerged from recent studies from the laboratory of Møller and colleagues that challenged the consensus idea that the elevation of cytosolic Ca^{2+}—rather than the depletion of ER Ca^{2+}—led to the cell death induced by thapsigargin and analogs (Sehgal et al., 2017; Szalai et al., 2018). Contrary to what is generally thought, the rapid rise of cytosolic Ca^{2+}, as observed with thapsigargin, and its role in the short-term side effect on cardiac contractility, is not required for apoptosis after SERCA inhibition. It is rather the ER Ca^{2+} depletion and sustained UPR activation that contributes to cell death (Sehgal et al., 2017).

The effect of a given SERCA inhibitor on cytosolic and ER Ca^{2+} levels depends strongly on its molecular mechanism of interaction with the ATPase. For example, the thapsigargin derivative substituted with a 12-aminododecanoyl linker, Boc-8ADT, did not show measurable changes in Ca^{2+} levels even though it strongly inhibited SERCA ATPase activity (Sehgal et al., 2017) leading to apoptosis in LNCaP cells (Dubois et al., 2013). This is probably due to the very slow binding kinetics of this compound leading to a slow net leakage of Ca^{2+} from the ER, which likely enables the maintenance of constant, stable cytosolic Ca^{2+} levels. Other possible causes for the lack of cytosolic Ca^{2+} peaks are a moderate decrease in SERCA's Ca^{2+} affinity or a residual Ca^{2+} transport activity in the presence of the compound. It is tempting to speculate that other SERCA inhibitors that have advanced to clinical testing might have a similar mode of action. Curcumin, a small molecule derived from the turmeric spice that stabilizes SERCA in the E1 conformational state has been extensively tested in multiple cancer models and clinical trials (Wilken et al., 2011) without causing major cardiac events. Cisplatin is a widely used platinum-containing compound that, among other effects, inhibits SERCA and Na^+/K^+-ATPase simultaneously (Tadini-Buoninsegni et al., 2017). Given the large number or rotating bonds in CAD204520, slow binding kinetics to SERCA, as with Boc-8ADT, can also be anticipated. From our structural data, the interaction of CAD204520 with SERCA involves only two polar contacts, and one single hydrophobic contact within a distance of 3 Å. Overall the interaction looks surprisingly "loose",

and fraction of shortening (C) (FS%), before and after the CAD204520 (5 μM) or thapsigargin (200 nM) treatment compared with control (Control). (A–C) Right panels: mean percentage effect of CAD204520 ($CAD204520_{2h}$) and thapsigargin ($Thapsigargin_{200nM}$) on the same cardiac functions. Graph bars: mean ± SD of the six CAD204520-treated cardiomyocyte groups and mean ± SD of the two thapsigargin-treated cardiomyocyte groups. Statistical significance comparing CAD204520-treated cells versus thapsigargin-treated cells (**$p \leq 0.001$, *$p \leq 0.05$) was determined by a non-parametric t test (Mann-Whitney).

(D) Effect of daily 30 mg/kg administration of CAD204520 on body weight. Error bars denote the mean ± SD of six replicates (three male and three female mice). Statistical significance (n.s.) was determined by a two-way ANOVA analysis.

(E) Effect of CAD204520 on T-ALL leukemia burden in an SKW-3/KE-37-xenografted murine model. Anti-leukemic activity of CAD204520 assessed by measuring $hCD45^+$ cells after 4 days of CAD204520 treatment (45 mg/kg/OS BID) or vehicle (Tween 80 0.5%, w/v, and hydroxypropyl-methylcellulose [HPMC] 1.0%, w/v). Representative dot plot showing the effect of CAD204520 on T-ALL growth in an SKW-3/KE-37 murine model. A minimum of 20,000 events was collected for each condition.

(F) Immunohistochemical analysis of the spleen in an SKW-3/KE-37-xenografted murine model treated with CAD204520 45 mg/kg or vehicle for 4 days. The spleens of all mice were examined; representative results for one control animal and one CAD204520-treated animal are shown. Formalin-fixed, paraffin-embedded tissue sections were stained with hCD45. Scale bars, 20 μm.

(G) Representative images of hematoxylin/eosin-stained sections of the left ventricle from SKW-3/KE-37 xenograft treated with CAD204520 45 mg/kg or vehicle. CAD204520 treatment did not affect the gross structural components of the myocardium or induce focal areas of damage. Well-aligned myofibers in the absence of myocytolytic necrosis or interstitial inflammatory infiltrates are shown at higher magnification (inset). Scale bars, 0.2 mm (low magnification) and 0.05 mm (high magnification; insets).

(H) Representative images of hematoxylin/eosin-stained histological sections of the small intestines from SKW-3/KE-37 xenograft treated with CAD204520 45 mg/kg or vehicle. Compared with controls, intestinal villi and crypts appear to be well preserved in CAD204520-treated animals. At higher magnification (inset), no morphological changes in goblet cells and enterocytes were observed in CAD204520-treated mice. Scale bars, 0.2 mm (low magnification) and 0.05 mm (high magnification; insets).

(I) Effect of CAD204520 on cell blood count WBC, hemoglobin, and platelets in an SKW-3/KE-37 murine model after 4 days of CAD204520 treatment (45 mg/kg/OS BID) or vehicle (Tween 80 0.5%, w/v, and HPMC 1.0%, w/v). Error bars denote the mean ± SD of eight CAD204520-treated animals or the mean ± SD of eight replicates vehicle-treated mice. Statistical significance for treated versus vehicle (n.s.) was determined by non-parametric t test (Mann-Whitney).

See also Figure S7.

perhaps indicating a concentration-dependent competition with Ca^{2+} binding and transport rather than an irreversible inhibition.

Our data also show that CAD204520 binds to SERCA differently from thapsigargin: it occupies a pocket between the transmembrane helices M1, M2, M3, and M4 of SERCA, whereas thapsigargin binds between M3, M5, and M7 (Brini and Carafoli, 2009). This observation agrees with our finding that thapsigargin, but not CPA, co-treatment enhances CAD204520's inhibitory effect, a feature that can be used for further medicinal chemistry optimization. In this regard, however, CAD204520 maintains the same thapsigargin "property" to preferentially alter mutated NOTCH1 trafficking. Remarkably, this ability has not yet been explored in two of the most recently synthesized putative SERCA inhibitors: the natural tricyclic clerodane diterpene casearin J (De Ford et al., 2016) or ethyl 2-amino-6-(3,5-dimethoxyphenyl)-4-(2-ethoxy-2-oxoethyl)-4H-chromene-3-carboxylate (CXL017) (Bleeker et al., 2013), both active in T-ALL cell lines.

The next question is whether CAD204520 activity has limitations *in vivo* due to Ca^{2+} shifts. For example, mice exposed to a thapsigargin analog, L12-ADT, at 0.8 mg/kg, die within 8 h, putatively from cardiac toxicity (Denmeade et al., 2003). Cardiac sarcoplasmic reticulum (SR) Ca^{2+} ATPase (SERCA2a) plays a central role in myocardial contractility. SERCA2a actively transports Ca^{2+} into the SR and regulates cytosolic Ca^{2+} concentration, SR Ca^{2+} load, and thus the rate of contraction and relaxation of the heart (Periasamy et al., 2008). The amount of Ca^{2+} release from the SR, dictating the extent of cell shortening, is also a steep function of SR Ca^{2+} content (Bassani et al., 1995). It follows that pharmacological inhibition of SERCA2a activity should reduce the amplitude of the transient calcium and the rate of SERCA-mediated Ca^{2+} removal, resulting in altered cardiomyocyte mechanics, as we observed in isolated unloaded ventricular myocytes exposed to CAD204520 or thapsigargin. However, the impairment of cellular contractile performance and Ca^{2+} dynamics was more pronounced after thapsigargin incubation compared with CAD204520 exposure (80%–90% reduction in functional performance versus 25%–30%, on average), indicating that CAD204520 should have a better therapeutic window than thapsigargin *in vivo*.

An important question is whether and to what extent the depressed cardiomyocyte function secondary to pharmacological inhibition of SERCA2 activity would translate into decreased cardiac function *in vivo*. Based on previous experience from our group in a rat model of induced cardiomyopathy (Savi et al., 2017), a 20%–30% decline in cellular mechanics *ex vivo* results in a comparable moderate hemodynamic impairment in the intact animal. In fact, while CAD204520 exerts an anti-leukemia effect *in vivo* it does not induce heart failure in the two different mouse models (BALB/c CD1 and IL2-NSG) used for this study.

Although most *NOTCH1* mutations are found in exons 26 and 27 coding for the HD region, mutations in the PEST domain are present in 20%–30% of tumors resulting in an increased Notch activation due to the prolonged stabilization of ICN1 (Weng et al., 2004). Activating mutations clustered in the PEST sequence have been described in CLL and in MCL, and several efforts are ongoing to target NOTCH1 in these diseases (Baldoni et al., 2018; Kridel et al., 2012). Our study demonstrates that CAD204520 is active in cell lines carrying a PEST mutation (SKW-3/KE-37). This result supports testing SERCA inhibitors in disease models with this recurrent abnormality, such as CLL (Di Ianni et al., 2009) and MCL (Kridel et al., 2012). To this end, we extended testing CAD204520 in the REC-1 MCL cell line, one of the few representative models of NOTCH1-dependent MCL (Kridel et al., 2012) carrying a H2428Pfs*7 PEST mutation. We showed that REC-1 is sensitive to CAD204520 inhibition compared with *NOTCH1* wild-type MCL lines. In REC-1, CAD204520 reduces Notch activation with a mechanism similar to the one observed in T-ALL. Because in MCL *NOTCH1* mutations are associated with significantly shorter survival rates (Bea et al., 2013; Kridel et al., 2012), the development of Notch-targeted therapy may represent an effective strategy to tackle this aggressive disease.

In conclusion, this study presents CAD204520 as an orally bioavailable SERCA inhibitor with tolerable off-target toxicity in NOTCH1-dependent tumors. This work provides a foundation for further development of novel drugs targeting Notch-dependent cancers. It also provides a deeper understanding of how different SERCA modulators affect cardiac tissue physiology.

SIGNIFICANCE

Given its critical oncogenic role in several human cancers, Notch1 signaling has garnered increased attention as a potential therapeutic target. To date, several Notch modulators, including γ-secretase inhibitors, have shown therapeutic efficacy in preclinical cancer models. However, despite this promise, few of these candidates have been demonstrated to have a meaningful clinical benefit for patients, in part due to tissue-dependent on-target toxicities from the simultaneous repression of both mutant and wild-type Notch proteins.

The discovery of SERCAs as actionable modulators of Notch1 suggested a targeted approach to treat NOTCH1-dependent cancer, including T-ALL, MCL, and CLL. Uniquely among Notch modulators, SERCA inhibitors preferentially impair the clinically relevant class of oncogenic *NOTCH1* mutants compared with wild type. Thus, the development of tolerated SERCA modulators may uncover a therapeutic avenue for one of the most frequently mutated genes in human cancers.

STAR★METHODS

Detailed methods are provided in the online version of this paper and include the following:

- KEY RESOURCES TABLE
- RESOURCE AVAILABILITY
  - Lead Contact
  - Materials Availability
- EXPERIMENTAL MODEL AND SUBJECT DETAILS
  - Animals
  - Yeast Cells
  - Cell Lines
  - Primary Samples
- DATA AND CODE AVAILABILITY

SUPPLEMENTAL INFORMATION

Supplemental Information can be found online at https://doi.org/10.1016/j.chembiol.2020.04.002.

ACKNOWLEDGMENTS

This work was supported by an AIRC Start-up Investigator Grant (no. 17107 to G.R.), Fondazione Cariparma (3576/2017 and 0180/2018 to G.R.), Fondazione Grande Ale Onlus (to G.R.), L'antica Torre di Melezzole (to M.M.), Fondazione Umberto Veronesi Post-doctoral Fellowship (to C.S.), Associazione Italiana contro le Leucemie-Linfomi e Mieloma ONLUS Parma chapter (to A.G.), AIRC Investigator Grant 2018 (no. 21352 to P.S.), the Italian Ministry of Education, University and Research (Programma SIR no. RBSI14GPBL to P.S.), Fondazione Cassa di Risparmio di Perugia (project code: 2018. 0418.021) and Gilead fellowship program 2019 (to R.L.S.), Progetti di Ricerca di Interesse Nazionale (PRIN) 2017 (project code: 2017PPS2X4 to C.M.), the National Cancer Institute R35 CA210030 and the Pan-Mass Challenge Team Crank (to K.S.). M.M. is a 2018 EHA-ASH Translational Training in Hematology scholar. The authors thank Federico Quaini, M.D., Ph.D., and Andrea Vecchi Ph.D., for technical assistance, Francesco Marchesini for art and design expertise, Antonio Cuneo, M.D., Ph.D., and Chiara Liverani, Ph.D., for critical suggestions, Sabrina Bonomini, Ph.D., and Gabriella Sammarrelli, Ph.D., for technical expertise, Niccolò Bolli, M.D., Ph.D., for sequencing oversight, and Pamela Criscuoli for administrative support, and the physicians at the Hematology and BMT unit of the University of Parma.

AUTHOR CONTRIBUTIONS

Conceptualization and Design, M.M., A.G., W.D.-B., A.-M.L.W., M.B., and G.R.; Methodology, all authors; Resources, all authors; Investigation, all authors; Formal Analysis, all authors; Writing – Original Draft, W.D.-B., A.-M.L.W., M.M., M.B., and G.R.; Writing – Review & Editing, W.D.-B., A.-M.L.W., M.M., M.B., and G.R.; Data Curation, W.D.-B., A.-M.L.W., P.S., R.L.S., C.M., F.A., K.S., M.B., and G.R. Funding Acquisition, P.S., C.M., R.L.S., K.S., M.M., and G.R.; Project Administration, M.M. and G.R.; Supervision, G.R.

DECLARATION OF INTERESTS

W.D.-B. and A.-M.L.W. are CaDo Biotechnology IvS employees. The compounds studied are part of a patent application wholly owned by CaDo Biotechnology IvS, Denmark. K.S. has previously consulted for Novartis and Rigel Pharmaceuticals and currently receives grant funding from Novartis on topics unrelated to this manuscript.

Received: July 4, 2019
Revised: February 14, 2020
Accepted: March 31, 2020
Published: May 7, 2020

REFERENCES

Abdullahi, A., Stanojcic, M., Parousis, A., Patsouris, D., and Jeschke, M.G. (2017). Modeling acute ER stress in vivo and in vitro. Shock *47*, 506–513.

Adams, P.D., Afonine, P.V., Bunkoczi, G., Chen, V.B., Davis, I.W., Echols, N., Headd, J.J., Hung, L.W., Kapral, G.J., Grosse-Kunstleve, R.W., et al. (2010). PHENIX: a comprehensive Python-based system for macromolecular structure solution. Acta Crystallogr. D Biol. Crystallogr. *66*, 213–221.

Andersen, J.P., Lassen, K., and Moller, J.V. (1985). Changes in Ca^{2+} affinity related to conformational transitions in the phosphorylated state of soluble monomeric Ca^{2+}-ATPase from sarcoplasmic reticulum. J. Biol. Chem. *260*, 371–380.

Andersen, T.B., Lopez, C.Q., Manczak, T., Martinez, K., and Simonsen, H.T. (2015). Thapsigargin—from *Thapsia* L. to mipsagargin. Molecules *20*, 6113–6127.

Arbabian, A., Brouland, J.P., Gelebart, P., Kovacs, T., Bobe, R., Enouf, J., and Papp, B. (2011). Endoplasmic reticulum calcium pumps and cancer. Biofactors *37*, 139–149.

Arruga, F., Gizdic, B., Serra, S., Vaisitti, T., Ciardullo, C., Coscia, M., Laurenti, L., D'Arena, G., Jaksic, O., Inghirami, G., et al. (2014). Functional impact of NOTCH1 mutations in chronic lymphocytic leukemia. Leukemia *28*, 1060–1070.

Artavanis-Tsakonas, S., Rand, M.D., and Lake, R.J. (1999). Notch signaling: cell fate control and signal integration in development. Science *284*, 770–776.

Aster, J.C., Pear, W.S., and Blacklow, S.C. (2008). Notch signaling in leukemia. Annu. Rev. Pathol. *3*, 587–613.

Baldoni, S., Del Papa, B., Dorillo, E., Aureli, P., De Falco, F., Rompietti, C., Sorcini, D., Varasano, E., Cecchini, D., Zei, T., et al. (2018). Bepridil exhibits anti-leukemic activity associated with NOTCH1 pathway inhibition in chronic lymphocytic leukemia. Int. J. Cancer *143*, 958–970.

Baliakas, P., Hadzidimitriou, A., Sutton, L.A., Rossi, D., Minga, E., Villamor, N., Larrayoz, M., Kminkova, J., Agathangelidis, A., Davis, Z., et al. (2015). Recurrent mutations refine prognosis in chronic lymphocytic leukemia. Leukemia *29*, 329–336.

Ball, M., Andrews, S.P., Wierschem, F., Cleator, E., Smith, M.D., and Ley, S.V. (2007). Total synthesis of thapsigargin, a potent SERCA pump inhibitor. Org. Lett. *9*, 663–666.

Bassani, J.W.M., Yuan, W.L., and Bers, D.M. (1995). Fractional Sr Ca release is regulated by trigger Ca and Sr Ca content in cardiac myocytes. Am. J. Physiol. Cell Physiol. *268*, C1313–C1319.

Bea, S., Valdes-Mas, R., Navarro, A., Salaverria, I., Martin-Garcia, D., Jares, P., Gine, E., Pinyol, M., Royo, C., Nadeu, F., et al. (2013). Landscape of somatic mutations and clonal evolution in mantle cell lymphoma. Proc. Natl. Acad. Sci. U S A *110*, 18250–18255.

Blaumueller, C.M., Qi, H., Zagouras, P., and Artavanis-Tsakonas, S. (1997). Intracellular cleavage of Notch leads to a heterodimeric receptor on the plasma membrane. Cell *90*, 281–291.

Bleeker, N.P., Cornea, R.L., Thomas, D.D., and Xing, C. (2013). A novel SERCA inhibitor demonstrates synergy with classic SERCA inhibitors and targets multidrug-resistant AML. Mol. Pharm. *10*, 4358–4366.

Bocchi, L., Savi, M., Naponelli, V., Vilella, R., Sgarbi, G., Baracca, A., Solaini, G., Bettuzzi, S., Rizzi, F., and Stilli, D. (2018). Long-term oral administration of theaphenon-E improves cardiomyocyte mechanics and calcium dynamics by affecting phospholamban phosphorylation and ATP production. Cell Physiol. Biochem. *47*, 1230–1243.

Brini, M., and Carafoli, E. (2009). Calcium pumps in health and disease. Physiol. Rev. *89*, 1341–1378.

Brzozowa-Zasada, M., Piecuch, A., Michalski, M., Segiet, O., Kurek, J., Harabin-Slowinska, M., and Wojnicz, R. (2017). Notch and its oncogenic activity in human malignancies. Eur. Surg. *49*, 199–209.

Bublitz, M., Kjellerup, L., Cohrt, K.O., Gordon, S., Mortensen, A.L., Clausen, J.D., Pallin, T.D., Hansen, J.B., Fuglsang, A.T., Dalby-Brown, W., and Winther, A.L. (2018). Tetrahydrocarbazoles are a novel class of potent P-type ATPase inhibitors with antifungal activity. PLoS One *13*, e0188620.

Bublitz, M., Morth, J.P., and Nissen, P. (2011). P-type ATPases at a glance. J. Cell Sci. *124*, 2515–2519.

Burghoorn, H.P., Soteropoulos, P., Paderu, P., Kashiwazaki, R., and Perlin, D.S. (2002). Molecular evaluation of the plasma membrane proton pump from *Aspergillus fumigatus*. Antimicrob. Agents Chemother. *46*, 615–624.

Chemaly, E.R., Troncone, L., and Lebeche, D. (2018). SERCA control of cell death and survival. Cell Calcium *69*, 46–61.

Chen, D., and Evans, P.A. (2017). A concise, efficient and scalable total synthesis of thapsigargin and nortrilobolide from (R)-(-)-carvone. J. Am. Chem. Soc. *139*, 6046–6049.

Chidawanyika, T., Sergison, E., Cole, M., Mark, K., and Supattapone, S. (2018). SEC24A identified as an essential mediator of thapsigargin-induced cell death in a genome-wide CRISPR/Cas9 screen. Cell Death Discov. *4*, 115.

Chou, T.C. (2010). Drug combination studies and their synergy quantification using the Chou-Talalay method. Cancer Res. *70*, 440–446.

Christensen, S.B., Andersen, A., Poulsen, J.C., and Treiman, M. (1993). Derivatives of thapsigargin as probes of its binding site on endoplasmic reticulum Ca^{2+} ATPase. Stereoselectivity and important functional groups. FEBS Lett. *335*, 345–348.

Christensen, S.B., Skytte, D.M., Denmeade, S.R., Dionne, C., Moller, J.V., Nissen, P., and Isaacs, J.T. (2009). A Trojan horse in drug development: targeting of thapsigargins towards prostate cancer cells. Anticancer Agents Med. Chem. *9*, 276–294.

Chu, H., Smith, J.M., Felding, J., and Baran, P.S. (2017). Scalable synthesis of (-)-thapsigargin. ACS Cent. Sci. *3*, 47–51.

Cid, A., Perona, R., and Serrano, R. (1987). Replacement of the promoter of the yeast plasma membrane ATPase gene by a galactose-dependent promoter and its physiological consequences. Curr. Genet. *12*, 105–110.

Clark, J.H., Kinnear, N.P., Kalujnaia, S., Cramb, G., Fleischer, S., Jeyakumar, L.H., Wuytack, F., and Evans, A.M. (2010). Identification of functionally segregated sarcoplasmic reticulum calcium stores in pulmonary arterial smooth muscle. J. Biol. Chem. *285*, 13542–13549.

Clausen, J.D., Kjellerup, L., Cohrt, K.O., Hansen, J.B., Dalby-Brown, W., and Winther, A.L. (2017). Elucidation of antimicrobial activity and mechanism of action by N-substituted carbazole derivatives. Bioorg. Med. Chem. Lett. *27*, 4564–4570.

Dally, S., Corvazier, E., Bredoux, R., Bobe, R., and Enouf, J. (2010). Multiple and diverse coexpression, location, and regulation of additional SERCA2 and SERCA3 isoforms in nonfailing and failing human heart. J. Mol. Cell Cardiol. *48*, 633–644.

Dally, S., Monceau, V., Corvazier, E., Bredoux, R., Raies, A., Bobe, R., del Monte, F., and Enouf, J. (2009). Compartmentalized expression of three novel sarco/endoplasmic reticulum Ca^{2+}ATPase 3 isoforms including the switch to ER stress, SERCA3f, in non-failing and failing human heart. Cell Calcium *45*, 144–154.

De Ford, C., Heidersdorf, B., Haun, F., Murillo, R., Friedrich, T., Borner, C., and Merfort, I. (2016). The clerodane diterpene casearin J induces apoptosis of T-ALL cells through SERCA inhibition, oxidative stress, and interference with Notch1 signaling. Cell Death Dis. *7*, e2070.

De Strooper, B., Annaert, W., Cupers, P., Saftig, P., Craessaerts, K., Mumm, J.S., Schroeter, E.H., Schrijvers, V., Wolfe, M.S., Ray, W.J., et al. (1999). A presenilin-1-dependent gamma-secretase-like protease mediates release of Notch intracellular domain. Nature *398*, 518–522.

DeAngelo, D.J., Stone, R.M., Silverman, L.B., and Aster, J.C. (2006). A phase I clinical trial of the Notch inhibitor MK-0752 in patients with T-cell acute lymphoblastic leukemia/lymphoma (T-ALL) and other leukemias. J. Clin. Oncol. *24*, 6585.

Denmeade, S.R., and Isaacs, J.T. (2005). The SERCA pump as a therapeutic target: making a "smart bomb" for prostate cancer. Cancer Biol. Ther. *4*, 14–22.

Denmeade, S.R., Jakobsen, C.M., Janssen, S., Khan, S.R., Garrett, E.S., Lilja, H., Christensen, S.B., and Isaacs, J.T. (2003). Prostate-specific antigen-activated thapsigargin prodrug as targeted therapy for prostate cancer. J. Natl. Cancer Inst. *95*, 990–1000.

Di Ianni, M., Baldoni, S., Rosati, E., Ciurnelli, R., Cavalli, L., Martelli, M.F., Marconi, P., Screpanti, I., and Falzetti, F. (2009). A new genetic lesion in B-CLL: a NOTCH1 PEST domain mutation. Br. J. Haematol. *146*, 689–691.

Doan, N.T., Paulsen, E.S., Sehgal, P., Moller, J.V., Nissen, P., Denmeade, S.R., Isaacs, J.T., Dionne, C.A., and Christensen, S.B. (2015). Targeting thapsigargin towards tumors. Steroids *97*, 2–7.

Doody, R.S., Raman, R., Sperling, R.A., Seimers, E., Sethuraman, G., Mohs, R., Farlow, M., Iwatsubo, T., Vellas, B., Sun, X., et al. (2015). Peripheral and central effects of gamma-secretase inhibition by semagacestat in Alzheimer's disease. Alzheimers Res. Ther. *7*, 36.

Drachmann, N.D., Olesen, C., Moller, J.V., Guo, Z., Nissen, P., and Bublitz, M. (2014). Comparing crystal structures of Ca(2+)-ATPase in the presence of different lipids. FEBS J. *281*, 4249–4262.

Dubois, C., Vanden Abeele, F., Sehgal, P., Olesen, C., Junker, S., Christensen, S.B., Prevarskaya, N., and Moller, J.V. (2013). Differential effects of thapsigargin analogues on apoptosis of prostate cancer cells: complex regulation by intracellular calcium. FEBS J. *280*, 5430–5440.

Ellisen, L.W., Bird, J., West, D.C., Soreng, A.L., Reynolds, T.C., Smith, S.D., and Sklar, J. (1991). TAN-1, the human homolog of the *Drosophila* notch gene, is broken by chromosomal translocations in T lymphoblastic neoplasms. Cell *66*, 649–661.

Emsley, P., and Cowtan, K. (2004). Coot: model-building tools for molecular graphics. Acta Crystallogr. D Biol. Crystallogr. *60*, 2126–2132.

Evans, P.R., and Murshudov, G.N. (2013). How good are my data and what is the resolution? Acta Crystallogr. D Biol. Crystallogr. *69*, 1204–1214.

Extance, A. (2010). Alzheimer's failure raises questions about disease-modifying strategies. Nat. Rev. Drug Discov. *9*, 749–751.

Follini, E., Marchesini, M., and Roti, G. (2019). Strategies to overcome resistance mechanisms in T-cell acute lymphoblastic leukemia. Int. J. Mol. Sci. *20*, https://doi.org/10.3390/ijms20123021.

Golde, T.E., Koo, E.H., Felsenstein, K.M., Osborne, B.A., and Miele, L. (2013). gamma-Secretase inhibitors and modulators. Biochim. Biophys. Acta *1828*, 2898–2907.

Groeneweg, J.W., DiGloria, C.M., Yuan, J., Richardson, W.S., Growdon, W.B., Sathyanarayanan, S., Foster, R., and Rueda, B.R. (2014). Inhibition of notch signaling in combination with Paclitaxel reduces platinum-resistant ovarian tumor growth. Front. Oncol. *4*, 171.

Hauptman, P.J., and Kelly, R.A. (1999). Digitalis. Circulation *99*, 1265–1270.

Hill, J.E., Myers, A.M., Koerner, T.J., and Tzagoloff, A. (1986). Yeast/*E. coli* shuttle vectors with multiple unique restriction sites. Yeast *2*, 163–167.

Horn, M., Kroef, V., Allmeroth, K., Schuller, N., Miethe, S., Peifer, M., Penninger, J.M., Elling, U., and Denzel, M.S. (2018). Unbiased compound-protein interface mapping and prediction of chemoresistance loci through forward genetics in haploid stem cells. Oncotarget *9*, 9838–9851.

Inamdar, A.A., Goy, A., Ayoub, N.M., Attia, C., Oton, L., Taruvai, V., Costales, M., Lin, Y.T., Pecora, A., and Suh, K.S. (2016). Mantle cell lymphoma in the era of precision medicine-diagnosis, biomarkers and therapeutic agents. Oncotarget *7*, 48692–48731.

Kabsch, W. (2010). Xds. Acta Crystallogr. D Biol. Crystallogr. *66*, 125–132.

Kjellerup, L., Gordon, S., Cohrt, K.O., Brown, W.D., Fuglsang, A.T., and Winther, A.L. (2017). Identification of antifungal H(+)-ATPase inhibitors with effect on plasma membrane potential. Antimicrob. Agents Chemother. *61*, https://doi.org/10.1128/AAC.00032-17.

Klinakis, A., Lobry, C., Abdel-Wahab, O., Oh, P., Haeno, H., Buonamici, S., van De Walle, I., Cathelin, S., Trimarchi, T., Araldi, E., et al. (2011). A novel tumour-suppressor function for the Notch pathway in myeloid leukaemia. Nature *473*, 230–233.

Klodos, I., Esmann, M., and Post, R.L. (2002). Large-scale preparation of sodium-potassium ATPase from kidney outer medulla. Kidney Int. *62*, 2097–2100.

Knoechel, B., Bhatt, A., Pan, L., Pedamallu, C.S., Severson, E., Gutierrez, A., Dorfman, D.M., Kuo, F.C., Kluk, M., Kung, A.L., et al. (2015). Complete hematologic response of early T-cell progenitor acute lymphoblastic leukemia to the gamma-secretase inhibitor BMS-906024: genetic and epigenetic findings in an outlier case. Cold Spring Harb Mol. Case Stud. *1*, a000539.

Kopan, R., and Ilagan, M.X. (2009). The canonical Notch signaling pathway: unfolding the activation mechanism. Cell *137*, 216–233.

Kridel, R., Meissner, B., Rogic, S., Boyle, M., Telenius, A., Woolcock, B., Gunawardana, J., Jenkins, C., Cochrane, C., Ben-Neriah, S., et al. (2012). Whole transcriptome sequencing reveals recurrent NOTCH1 mutations in mantle cell lymphoma. Blood *119*, 1963–1971.

La Starza, R., Barba, G., Demeyer, S., Pierini, V., Di Giacomo, D., Gianfelici, V., Schwab, C., Matteucci, C., Vicente, C., Cools, J., et al. (2016). Deletions of the long arm of chromosome 5 define subgroups of T-cell acute lymphoblastic leukemia. Haematologica *101*, 951–958.

La Starza, R., Borga, C., Barba, G., Pierini, V., Schwab, C., Matteucci, C., Lema Fernandez, A.G., Leszl, A., Cazzaniga, G., Chiaretti, S., et al. (2014). Genetic profile of T-cell acute lymphoblastic leukemias with MYC translocations. Blood *124*, 3577–3582.

Laursen, M., Bublitz, M., Moncoq, K., Olesen, C., Møller, J.V., Young, H.S., Nissen, P., and Morth, J.P. (2009). Cyclopiazonic acid is complexed to a divalent metal ion when bound to the sarcoplasmic reticulum Ca2+-ATPase. J. Biol. Chem. *284*, 13513–13518.

Lawrence, M.S., Stojanov, P., Mermel, C.H., Robinson, J.T., Garraway, L.A., Golub, T.R., Meyerson, M., Gabriel, S.B., Lander, E.S., and Getz, G. (2014). Discovery and saturation analysis of cancer genes across 21 tumour types. Nature *505*, 495–501.

Le Borgne, R. (2006). Regulation of Notch signalling by endocytosis and endosomal sorting. Curr. Opin. Cell Biol. *18*, 213–222.

Ley, S.V., Antonello, A., Balskus, E.P., Booth, D.T., Christensen, S.B., Cleator, E., Gold, H., Hogenauer, K., Hunger, U., Myers, R.M., et al. (2004). Synthesis of the thapsigargins. Proc. Natl. Acad. Sci. U S A *101*, 12073–12078.

Li, Z.H., Qiu, M.Z., Zeng, Z.L., Luo, H.Y., Wu, W.J., Wang, F., Wang, Z.Q., Zhang, D.S., Li, Y.H., and Xu, R.H. (2012). Copper-transporting P-type adenosine triphosphatase (ATP7A) is associated with platinum-resistance in non-small cell lung cancer (NSCLC). J. Transl. Med. *10*, 21.

Lipskaia, L., Chemaly, E.R., Hadri, L., Lompre, A.M., and Hajjar, R.J. (2010). Sarcoplasmic reticulum Ca(2+) ATPase as a therapeutic target for heart failure. Expert Opin. Biol. Ther. *10*, 29–41.

Litzow, M.R., and Ferrando, A.A. (2015). How I treat T-cell acute lymphoblastic leukemia in adults. Blood *126*, 833–841.

Liu, M., and Dudley, S.C., Jr. (2015). Role for the unfolded protein response in heart disease and cardiac arrhythmias. Int. J. Mol. Sci. *17*, https://doi.org/10.3390/ijms17010052.

Lobry, C., Oh, P., and Aifantis, I. (2011). Oncogenic and tumor suppressor functions of Notch in cancer: it's NOTCH what you think. J. Exp. Med. *208*, 1931–1935.

Loewe, S. (1953). The problem of synergism and antagonism of combined drugs. Arzneimittelforschung *3*, 285–290.

Logeat, F., Bessia, C., Brou, C., LeBail, O., Jarriault, S., Seidah, N.G., and Israel, A. (1998). The Notch1 receptor is cleaved constitutively by a furin-like convertase. Proc. Natl. Acad. Sci. U S A *95*, 8108–8112.

Lu, M., Lawrence, D.A., Marsters, S., Acosta-Alvear, D., Kimmig, P., Mendez, A.S., Paton, A.W., Paton, J.C., Walter, P., and Ashkenazi, A. (2014). Opposing unfolded-protein-response signals converge on death receptor 5 to control apoptosis. Science *345*, 98–101.

Lytton, J., Westlin, M., and Hanley, M.R. (1991). Thapsigargin inhibits the sarcoplasmic or endoplasmic reticulum Ca-ATPase family of calcium pumps. J. Biol. Chem. *266*, 17067–17071.

Ma, Z., Fan, C., Yang, Y., Di, S., Hu, W., Li, T., Zhu, Y., Han, J., Xin, Z., Wu, G., et al. (2016). Thapsigargin sensitizes human esophageal cancer to TRAIL-induced apoptosis via AMPK activation. Sci. Rep. *6*, 35196.

Mahalingam, D., Cetnar, J., Wilding, G., Denmeade, S., Sarantopoulos, J., Kurman, M., and Carducci, M. (2013). Abstract B244: a first-in-human phase 1 clinical study of G-202, a thapsigargin-based prostate-specific membrane antigen (PSMA) activated prodrug, in patients with advanced solid tumors. Mol. Cancer Ther. *12*, B244.

Mahalingam, D., Wilding, G., Denmeade, S., Sarantopoulas, J., Cosgrove, D., Cetnar, J., Azad, N., Bruce, J., Kurman, M., Allgood, V.E., and Carducci, M. (2016). Mipsagargin, a novel thapsigargin-based PSMA-activated prodrug: results of a first-in-man phase I clinical trial in patients with refractory, advanced or metastatic solid tumours. Br. J. Cancer *114*, 986–994.

Marks, D.I., and Rowntree, C. (2017). Management of adults with T-cell lymphoblastic leukemia. Blood *129*, 1134–1142.

McCoy, A.J. (2007). Solving structures of protein complexes by molecular replacement with Phaser. Acta Crystallogr. D Biol. Crystallogr. *63*, 32–41.

Meraviglia, V., Bocchi, L., Sacchetto, R., Florio, M.C., Motta, B.M., Corti, C., Weichenberger, C.X., Savi, M., D'Elia, Y., Rosato-Siri, M.D., et al. (2018). HDAC inhibition improves the sarcoendoplasmic reticulum Ca(2+)-ATPase activity in cardiac myocytes. Int. J. Mol. Sci. *19*, https://doi.org/10.3390/ijms19020419.

Minowada, J., Kohno, K., Matsuo, Y., Drexler, H.G., Ohnuma, T., Tax, W.J., and Brenner, M.B. (1989). Characteristics of 27 human T-cell leukemia cell lines with/without T-cell receptors of T3-Ti alpha beta or T3-Ti gamma delta complex. Haematol. Blood Transfus. *32*, 233–236.

Mukherjee, N., Almeida, A., Partyka, K.A., Lu, Y., Schwan, J.V., Lambert, K., Rogers, M., Robinson, W.A., Robinson, S.E., Applegate, A.J., et al. (2016). Combining a GSI and BCL-2 inhibitor to overcome melanoma's resistance to current treatments. Oncotarget *7*, 84594–84607.

Obara, K., Miyashita, N., Xu, C., Toyoshima, I., Sugita, Y., Inesi, G., and Toyoshima, C. (2005). Structural role of countertransport revealed in Ca2+ pump crystal structure in the absence of Ca2+. PNAS *102*, 14489–14496.

Orrenius, S., Zhivotovsky, B., and Nicotera, P. (2003). Regulation of cell death: the calcium-apoptosis link. Nat. Rev. Mol. Cell Biol. *4*, 552–565.

Palomero, T., Lim, W.K., Odom, D.T., Sulis, M.L., Real, P.J., Margolin, A., Barnes, K.C., O'Neil, J., Neuberg, D., Weng, A.P., et al. (2006). NOTCH1 directly regulates c-MYC and activates a feed-forward-loop transcriptional network promoting leukemic cell growth. Proc. Natl. Acad. Sci. U S A *103*, 18261–18266.

Parekh, A.B., and Putney, J.W., Jr. (2005). Store-operated calcium channels. Physiol. Rev. *85*, 757–810.

Penton, A.L., Leonard, L.D., and Spinner, N.B. (2012). Notch signaling in human development and disease. Semin. Cell Dev. Biol. *23*, 450–457.

Periasamy, M., Bhupathy, P., and Babu, G.J. (2008). Regulation of sarcoplasmic reticulum Ca^{2+} ATPase pump expression and its relevance to cardiac muscle physiology and pathology. Cardiovasc. Res. *77*, 265–273.

Puente, X.S., Pinyol, M., Quesada, V., Conde, L., Ordonez, G.R., Villamor, N., Escaramis, G., Jares, P., Bea, S., Gonzalez-Diaz, M., et al. (2011). Whole-genome sequencing identifies recurrent mutations in chronic lymphocytic leukaemia. Nature *475*, 101–105.

Pui, J.C., Allman, D., Xu, L., DeRocco, S., Karnell, F.G., Bakkour, S., Lee, J.Y., Kadesch, T., Hardy, R.R., Aster, J.C., and Pear, W.S. (1999). Notch1 expression in early lymphopoiesis influences B versus T lineage determination. Immunity *11*, 299–308.

Quynh Doan, N.T., and Christensen, S.B. (2015). Thapsigargin, origin, chemistry, structure-activity relationships and prodrug development. Curr. Pharm. Des. *21*, 5501–5517.

Riccio, O., van Gijn, M.E., Bezdek, A.C., Pellegrinet, L., van Es, J.H., Zimber-Strobl, U., Strobl, L.J., Honjo, T., Clevers, H., and Radtke, F. (2008). Loss of

intestinal crypt progenitor cells owing to inactivation of both Notch1 and Notch2 is accompanied by derepression of CDK inhibitors p27Kip1 and p57Kip2. EMBO Rep. *9*, 377–383.

Roti, G., Carlton, A., Ross, K.N., Markstein, M., Pajcini, K., Su, A.H., Perrimon, N., Pear, W.S., Kung, A.L., Blacklow, S.C., et al. (2013). Complementary genomic screens identify SERCA as a therapeutic target in NOTCH1 mutated cancer. Cancer Cell *23*, 390–405.

Roti, G., Qi, J., Kitara, S., Sanchez-Martin, M., Saur Conway, A., Varca, A.C., Su, A., Wu, L., Kung, A.L., Ferrando, A.A., et al. (2017). Leukemia-specific delivery of mutant NOTCH1 targeted therapy. J. Exp. Med. *215*, 197–216.

Roti, G., and Stegmaier, K. (2011). Targeting NOTCH1 in hematopoietic malignancy. Crit. Rev. Oncog. *16*, 103–115.

Roti, G., and Stegmaier, K. (2014). New approaches to target T-ALL. Front. Oncol. *4*, 170.

Roy, M., Pear, W.S., and Aster, J.C. (2007). The multifaceted role of Notch in cancer. Curr. Opin. Genet. Dev. *17*, 52–59.

Sachs, G. (1997). Proton pump inhibitors and acid-related diseases. Pharmacotherapy *17*, 22–37.

Samimi, G., Safaei, R., Katano, K., Holzer, A.K., Rochdi, M., Tomioka, M., Goodman, M., and Howell, S.B. (2004). Increased expression of the copper efflux transporter ATP7A mediates resistance to cisplatin, carboplatin, and oxaliplatin in ovarian cancer cells. Clin. Cancer Res. *10*, 4661–4669.

Savi, M., Bocchi, L., Mena, P., Dall'Asta, M., Crozier, A., Brighenti, F., Stilli, D., and Del Rio, D. (2017). In vivo administration of urolithin A and B prevents the occurrence of cardiac dysfunction in streptozotocin-induced diabetic rats. Cardiovasc. Diabetol. *16*, https://doi.org/10.1186/s12933-017-0561-3.

Schmitz, R., Wright, G.W., Huang, D.W., Johnson, C.A., Phelan, J.D., Wang, J.Q., Roulland, S., Kasbekar, M., Young, R.M., Shaffer, A.L., et al. (2018). Genetics and pathogenesis of diffuse large B-cell lymphoma. N. Engl. J. Med. *378*, 1396–1407.

Schott, A.F., Landis, M.D., Dontu, G., Griffith, K.A., Layman, R.M., Krop, I., Paskett, L.A., Wong, H., Dobrolecki, L.E., Lewis, M.T., et al. (2013). Preclinical and clinical studies of gamma secretase inhibitors with docetaxel on human breast tumors. Clin. Cancer Res. *19*, 1512–1524.

Sehgal, P., Szalai, P., Olesen, C., Praetorius, H.A., Nissen, P., Christensen, S.B., Engedal, N., and Moller, J.V. (2017). Inhibition of the sarco/endoplasmic reticulum (ER) Ca(2+)-ATPase by thapsigargin analogs induces cell death via ER Ca(2+) depletion and the unfolded protein response. J. Biol. Chem. *292*, 19656–19673.

Seto-Young, D., Monk, B., Mason, A.B., and Perlin, D.S. (1997). Exploring an antifungal target in the plasma membrane H(+)-ATPase of fungi. Biochim. Biophys. Acta *1326*, 249–256.

Sharma, A., Gadkari, R.A., Ramakanth, S.V., Padmanabhan, K., Madhumathi, D.S., Devi, L., Appaji, L., Aster, J.C., Rangarajan, A., and Dighe, R.R. (2015). A novel monoclonal antibody against Notch1 targets leukemia-associated mutant notch1 and depletes therapy resistant cancer stem cells in solid tumors. Sci. Rep. *5*, 11012.

Sorrentino, C., Cuneo, A., and Roti, G. (2019). Therapeutic targeting of notch signaling pathway in hematological malignancies. Mediterr. J. Hematol. Infect. Dis. *11*, e2019037.

Sovolyova, N., Healy, S., Samali, A., and Logue, S.E. (2014). Stressed to death—mechanisms of ER stress-induced cell death. Biol. Chem. *395*, 1–13.

Starza, R.L., Cambò, B., Pierini, A., Bornhauser, B., Montanaro, A., Bourquin, J.-P., Mecucci, C., and Roti, G. (2019). Venetoclax and bortezomib in relapsed/refractory early T-cell precursor acute lymphoblastic leukemia. JCO Precision Oncol. 1–6.

Stransky, N., Egloff, A.M., Tward, A.D., Kostic, A.D., Cibulskis, K., Sivachenko, A., Kryukov, G.V., Lawrence, M.S., Sougnez, C., McKenna, A., et al. (2011). The mutational landscape of head and neck squamous cell carcinoma. Science *333*, 1157–1160.

Szalai, P., Parys, J.B., Bultynck, G., Christensen, S.B., Nissen, P., Moller, J.V., and Engedal, N. (2018). Nonlinear relationship between ER Ca(2+) depletion versus induction of the unfolded protein response, autophagy inhibition, and cell death. Cell Calcium *76*, 48–61.

Tadini-Buoninsegni, F., Sordi, G., Smeazzetto, S., Natile, G., and Arnesano, F. (2017). Effect of cisplatin on the transport activity of PII-type ATPases. Metallomics *9*, 960–968.

Treiman, M., Caspersen, C., and Christensen, S.B. (1998). A tool coming of age: thapsigargin as an inhibitor of sarco-endoplasmic reticulum Ca(2+)-ATPases. Trends Pharmacol. Sci. *19*, 131–135.

Twarog, N.R., Stewart, E., Hammill, C.V., and Shelat, A.A. (2016). BRAID: a unifying paradigm for the analysis of combined drug action. Sci. Rep. *6*, 25523.

Twarog, N.R., Stewart, E., Hammill, C.V., and Shelat, A.A. (2018). Erratum: BRAID: a unifying paradigm for the analysis of combined drug action. Sci. Rep. *8*, 46970.

van Es, J.H., van Gijn, M.E., Riccio, O., van den Born, M., Vooijs, M., Begthel, H., Cozijnsen, M., Robine, S., Winton, D.J., Radtke, F., and Clevers, H. (2005). Notch/gamma-secretase inhibition turns proliferative cells in intestinal crypts and adenomas into goblet cells. Nature *435*, 959–963.

Wang, K., Li, M., and Hakonarson, H. (2010). ANNOVAR: functional annotation of genetic variants from high-throughput sequencing data. Nucleic Acids Res. *38*, e164.

Wang, M., and Kaufman, R.J. (2014). The impact of the endoplasmic reticulum protein-folding environment on cancer development. Nat. Rev. Cancer *14*, 581–597.

Wang, Z., Da Silva, T.G., Jin, K., Han, X., Ranganathan, P., Zhu, X., Sanchez-Mejias, A., Bai, F., Li, B., Fei, D.L., et al. (2014). Notch signaling drives stemness and tumorigenicity of esophageal adenocarcinoma. Cancer Res. *74*, 6364–6374.

Weng, A.P., Ferrando, A.A., Lee, W., Morris, J.P.t., Silverman, L.B., Sanchez-Irizarry, C., Blacklow, S.C., Look, A.T., and Aster, J.C. (2004). Activating mutations of NOTCH1 in human T cell acute lymphoblastic leukemia. Science *306*, 269–271.

Wilken, R., Veena, M.S., Wang, M.B., and Srivatsan, E.S. (2011). Curcumin: a review of anti-cancer properties and therapeutic activity in head and neck squamous cell carcinoma. Mol. Cancer *10*, 12.

Winther, A.M., Bublitz, M., Karlsen, J.L., Moller, J.V., Hansen, J.B., Nissen, P., and Buch-Pedersen, M.J. (2013). The sarcolipin-bound calcium pump stabilizes calcium sites exposed to the cytoplasm. Nature *495*, 265–269.

Yano, M., Ikeda, Y., and Matsuzaki, M. (2005). Altered intracellular Ca^{2+} handling in heart failure. J. Clin. Invest. *115*, 556–564.

Yatime, L., Buch-Pedersen, M.J., Musgaard, M., Morth, J.P., Lund Winther, A.M., Pedersen, B.P., Olesen, C., Andersen, J.P., Vilsen, B., Schiott, B., et al. (2009). P-type ATPases as drug targets: tools for medicine and science. Biochim. Biophys. Acta *1787*, 207–220.

Yu, M., Lin, J., Khadeer, M., Yeh, Y., Inesi, G., and Hussain, A. (1999). Effects of various amino acid 256 mutations on sarcoplasmic/endoplasmic reticulum Ca^{2+} ATPase function and their role in the cellular adaptive response to thapsigargin. Arch. Biochem. Biophys. *362*, 225–232.

Yu, M., Zhong, L., Rishi, A.K., Khadeer, M., Inesi, G., and Hussain, A. (1998). Specific substitutions at amino acid 256 of the sarcoplasmic/endoplasmic reticulum Ca^{2+} transport ATPase mediate resistance to thapsigargin in thapsigargin-resistant hamster cells. J. Biol. Chem. *273*, 3542–3546.

Yuan, X., Wu, H., Xu, H., Xiong, H., Chu, Q., Yu, S., Wu, G.S., and Wu, K. (2015). Notch signaling: an emerging therapeutic target for cancer treatment. Cancer Lett. *369*, 20–27.

Zhong, L., and Inesi, G. (1998). Role of the S3 stalk segment in the thapsigargin concentration dependence of sarco-endoplasmic reticulum Ca^{2+} ATPase inhibition. J. Biol. Chem. *273*, 12994–12998.

Please cite this article in press as: Marchesini et al., Blockade of Oncogenic NOTCH1 with the SERCA Inhibitor CAD204520 in T Cell Acute Lymphoblastic Leukemia, Cell Chemical Biology (2020), https://doi.org/10.1016/j.chembiol.2020.04.002

STAR★METHODS

KEY RESOURCES TABLE

REAGENT or RESOURCE	SOURCE	IDENTIFIER
Antibodies		
Rabbit monoclonal anti-Cleaved NOTCH1 (Val1744) (D3B8)	Cell Signaling	Cat# 4147; RRID: AB_2153348
Rabbit polyclonal anti-Cleaved NOTCH1 (Val1744)	Cell Signaling	Cat# 2421; RRID: AB_2314204
Goat polyclonal anti-NOTCH1 (C20)	Santa Cruz	Cat# sc-6014; RRID: AB_650336
Mouse monoclonal anti-NOTCH1	R&D Systems	Cat# FAB5317P; RRID: AB_1602927
Mouse monoclonal anti-NOTCH1 (A6)	Abcam	Cat# ab44986; RRID: AB_776840
Rabbit polyclonal anti-Cleaved PARP (Asp214)	Cell Signaling	Cat# 9541; RRID: AB_331427
Mouse monoclonal anti-β-Actin (8H10D10)	Cell Signaling	Cat# 3700; RRID: AB_2242334
Mouse monoclonal anti-GADPH (A3)	Santa Cruz	Cat# sc-137179; RRID: AB_2232048
Mouse monoclonal anti-HSP90 (4F-10)	Santa Cruz	Cat# sc-69703; RRID: AB_2121191
Rabbit monoclonal anti-SERCA2 (D51B11)	Cell Signaling	Cat# 9580
Mouse monoclonal anti-SERCA3 (PL/IM430)	Santa Cruz	Cat# sc-81759; RRID: AB_1129372
Rabbit monoclonal anti-BIP (C50B12)	Cell Signaling	Cat# 3177; RRID: AB_2119845
Rabbit polyclonal anti-phospho eIF2α (Ser51)	Cell Signaling	Cat# 9721; RRID: AB_330951
Rabbit polyclonal anti-eIF2α	Cell Signaling	Cat# 9722; RRID: AB_2230924
Mouse polyclonal anti-GOLGA1	Sigma-Aldrich	Cat# SAB1409131
Rabbit polyclonal anti-ATF6	Abcam	Cat# ab37149; RRID: AB_725571
Mouse monoclonal anti-human CD45 PE(HI30)	BD Biosciences	Cat# 560975; RRID: AB_2033960
Mouse monoclonal anti-human CD45 leucocyte common antigen (2B11+PD7/26)	Agilent	Cat# IS75130; RRID: AB_2661839
Goat polyclonal anti-Mouse IgG IRDye 680LT	LI-COR	Cat# 925-68020; RRID: AB_2687826
Goat polyclonal anti-Rabbit IgG IRDye 800CW	LI-COR	Cat# 925-32211; RRID: AB_2651127
Goat polyclonal anti-Rabbit IgG IRDye 680RD	LI-COR	Cat# 925-68071; RRID: AB_2721181
Goat polyclonal anti-Mouse IgG Alexa Fluor 488	Invitrogen	Cat# A-11029; RRID: AB_138404
Goat polyclonal anti-Rabbit IgG Alexa Fluor 568	Invitrogen	Cat# A-11036; RRID: AB_143011
Bacterial and Virus Strains		
pCMV-VSV-G packaging vector	Addgene	Cat# 8454; RRID: Addgene_8454
pCMV-delta R8.91	Laboratory of Kimberley Stegmaier (DFCI/Broad)	N/A
pXPR-011 expressing vector	Addgene	Cat# 59702; RRID: Addgene_59702
Biological Samples		
Primary samples	This paper	Parma and Perugia University Hospitals

(*Continued on next page*)

Continued

REAGENT or RESOURCE	SOURCE	IDENTIFIER
Chemicals, Peptides, and Recombinant Proteins		
Rabbit sarcoplasmic reticulum membranes	Andersen et al., 1985	N/A
Tris	Sigma-Aldrich	Cat# 252859
MOPS	Sigma-Aldrich	Cat# M1254
KCl	Sigma-Aldrich	Cat# P3911
$MgCl_2$	Sigma-Aldrich	Cat# 208377
$MgSO_4$	Sigma-Aldrich	Cat# 746452
$CaCl_2$	Sigma-Aldrich	Cat# C1016
NaOH	Sigma-Aldrich	Cat# S8045
NaCl	Sigma-Aldrich	Cat# S9888
NaN_3	Sigma-Aldrich	Cat# 71289
Na_2MoO_4	Sigma-Aldrich	Cat# 243655
$NaAsO_2$	Sigma-Aldrich	Cat# S7400
NaH_2PO_4	Sigma-Aldrich	Cat# S3139
$NaHCO_3$	Sigma-Aldrich	Cat# S6014
Sodium citrate dehydrate	Sigma-Aldrich	Cat# W302600
Sodium DOC	Sigma-Aldrich	Cat# D6750
Sodium pyruvate	Sigma-Aldrich	Cat# P8574
KNO_3	Sigma-Aldrich	Cat# P8394
K_2CO_3	Sigma-Aldrich	Cat# P5833
PtO_2	Sigma-Aldrich	Cat# 206032
2-bromopyridine	Sigma-Aldrich	Cat# B80100
EGTA	Sigma-Aldrich	Cat# E3889
HEPES	Sigma-Aldrich	Cat# 54457
Glycerol	Sigma-Aldrich	Cat# G7893
TNP-ATP	Sigma-Aldrich	Cat# SLM07040
C12E8	Sigma-Aldrich	Cat# P8925
PEG	Sigma-Aldrich	Cat# 8074911000
MPD	Sigma-Aldrich	Cat# 112100
DMF	Sigma-Aldrich	Cat# 227056
Ammonium heptamolybdate tetrahydrate	Sigma-Aldrich	Cat# 431346
Glacial acetic acid	Merk	Cat# 1005706
L-Ascorbic acid	Sigma-Aldrich	Cat# A5960
Dextrose	Sigma-Aldrich	Cat# D8066
Triton X-100	Sigma-Aldrich	Cat# T9284
Tween-80	Sigma-Aldrich	Cat# P1754
Taurine	Sigma-Aldrich	Cat# T0625
CuI	Sigma-Aldrich	Cat# 03140
Creatine	Sigma-Aldrich	Cat# C0780
Collagenase type II	Worthington Biochemical	Cat# LS004194
Protease type XIV	Sigma-Aldrich	Cat# P5147
DCM	Sigma-Aldrich	Cat# 4104976
DIPEA	Sigma-Aldrich	Cat# 03439
Ethanol	Sigma-Aldrich	Cat# 443611
Ethyl acetate	Sigma-Aldrich	Cat# 270989
Methanol	Sigma-Aldrich	Cat# 34860
CH_3CN	Sigma-Aldrich	Cat# L010010

(*Continued on next page*)

Continued

REAGENT or RESOURCE	SOURCE	IDENTIFIER
Dichloromethane	Supelco	Cat# DX0831
Triethylamine	Sigma-Aldrich	Cat# 90335
Paraformaldehyde 4%	ThermoFisher Scientific	Cat# 28908
Diethyl ether	Supelco	Cat# 1070625000
NMP	Sigma-Aldrich	Cat# 238634
MDAP	Sigma-Aldrich	Cat# 03439
Sarco/Endoplasmatic reticulum (SR) membranes	Claus E. Olesen and Jesper V. Møller, Aarhus University	N/A
Pig kidney Na^+, K^+-ATPase	Natalya Fedosova, Aarhus University	N/A
Fetal bovine serume (FBS)	ThermoFisher Scientific	Cat# MT10270-106
RPMI 1640	ThermoFisher Scientific	Cat# MT10040CV
Dulbecco's modified eagle medium (DMEM)	ThermoFisher Scientific	Cat# 11965-084
Claycomb medium	Sigma-Aldrich	Cat# 51800C
Penicillin-streptomycine	ThermoFisher Scientific	Cat# 3MT30002CI
L-Glutamine	ThermoFisher Scientific	Cat# 25030081
Norepinephrine [(±)- Arterenol]	Sigma-Aldrich	Cat# A0937
L-Ascorbic acid	Sigma-Aldrich	Cat# A7506
Gelatine from bovine skin	Sigma-Aldrich	Cat# G9391
Fibronectine bovine plasma	Sigma-Aldrich	Cat# F1141
DMSO	Sigma-Aldrich	Cat# 276855
Hydroxypropyl-methylcellulose (HPMC)	Shin-Etsu Chemical Co	Cat# SR-44439
Hematoxylin	Sigma-Aldrich	Cat# H3136
Eosin Y dye	Sigma-Aldrich	Cat# E4009
DAPT	Selleckchem	Cat# S2215
Thapsigargin	Enzo Biochem, Inc.	Cat# BML-PE180-0005
CAD204520	CaDo Biotechnology Ivs	N/A
DAPI	Sigma-Aldrich	Cat# D9542
FLUO3 AM	Invitrogen	Cat# F1241
Propidium iodide	Sigma-Aldrich	Cat# P4170
Indo1 AM	ThermoFisher Scientific	Cat# 1223
Critical Commercial Assays		
ATP-lite assay	PerkinElmer	Cat# 6016943
DC protein assay kit	Bio-Rad	Cat# 5000111
CellTiter-Glo ATP assay	Promega Corporation	Cat# G7573
Annexin V Apoptosis Detection Kit APC	eBioscience	Cat# 88-8007-74
LIVE/DEAD Fixable Far Red Dead Cell Stain	Invitrogen	Cat# L34973
Promega Maxwell® kit	Promega Corporation	Cat# AS1010
Agilent SureSelect Human all exon kit	Agilent Technologies	N/A
AMPure XP system	Beckman Coulter	N/A
Agilent high sensitivity DNA assay	Agilent Technologies	N/A
FuGENE 6 protocol	Promega Corporation	Cat# E2691
Deposited Data		
SERCA-Tg complex, molecular replacement model	Drachmann et al., 2014	PDB: 4UU0
SERCA-CAD204520 complex structure	This study	PDB: 6YAA

(*Continued on next page*)

Continued

REAGENT or RESOURCE	SOURCE	IDENTIFIER
Experimental Models: Cell Lines		
DND-41	DMSZ	Cat# ACC-525; RRID: CVCL_2022
MOLT16	DMSZ	Cat# ACC-29; RRID: CVCL_1424
REC-1	DMSZ	Cat# ACC-584; RRID: CVCL_1884
Mino	DMSZ	Cat# ACC-687; RRID: CVCL_1872
PF382	DMSZ	Cat# ACC-38; RRID: CVCL_1641
RPMI-8402	DMSZ	Cat# ACC-290; RRID: CVCL_1667
SKW-3/KE-37	DMSZ	Cat# ACC-53; RRID: CVCL_2197
CTV-1	DMSZ	Cat# ACC-40; RRID: CVCL_1150
Loucy	DMSZ	Cat# ACC-394; RRID: CVCL_1380
PEER	DMSZ	Cat# ACC-6; RRID: CVCL_1913
HSB2 (CCRF-HSB-2)	DMSZ	Cat# ACC-435; RRID: CVCL_1859
ALL/SIL	Laboratory of Kimberley Stegmaier (DFCI/Broad)	N/A
ALL/SIL thapsigargin resistant	This paper	University of Parma
MAVER-1	Laboratory of Elena Muraro (C.R.O., National Cancer Institute, Aviano, Italy)	N/A
293T (HEK293T)	DMSZ	Cat# ACC-635; RRID: CVCL_0063
HL-1	Laboratory of Michele Miragoli (University of Parma, Parma, Italy)	N/A
Experimental Models: Organisms/Strains		
Mouse: Crl: CD1(ICR) Mus Musculus	Aurigene	N/A
Mouse: BALB/cAnNCrl Mus Musculus	Aurigene	N/A
Mouse: NOD-*scid* IL2Rgamma^{null} Mus Musculus	The Jackson labs	Cat# 005557; RRID: IMSR_JAX:005557
Rat: Wistar Rattus Norvegicus	Charles River Laboratories	Cat# 13508588; RRID: RGD_13508588
Yeast: Saccharomyces cerevisiae RS72	ATCC	Cat# 9763
Oligonucleotides		
RT-PCR Primers for *RPL13A* gene	Applied Biosystems	Cat# Hs01926559_g1
RT-PCR Primers for *Myc* gene	Applied Biosystems	Cat# Hs00153401_m1
RT-PCR Primers for *DTX1* gene	Applied Biosystems	Cat# Hs00269995_m1
Software and Algorithms		
XDS	Kabsch, 2010	http://xds.mpimf-heidelberg.mpg.de/
AIMLESS	Evans and Murshudov, 2013	http://www.ccp4.ac.uk/html/aimless.html
PHASER	McCoy, 2007	http://www.phaser.com/
PHENIX	Adams et al., 2010	https://www.phenix-online.org/
Pymol Version 2.0	Molecular Graphics System, Schrödinger, LLC	https://pymol.org/2/
GraphPad Prism Version 7.0a	GraphPad Software Inc.	https://www.graphpad.com/scientific-software/prism/

(*Continued on next page*)

Continued

REAGENT or RESOURCE	SOURCE	IDENTIFIER
ImageJ Version 1.52q	NIH	http://rsbweb.nih.gov/ij/
FlowJo Version10	Tree Star LLC	https://www.flowjo.com/
SAMtool	Genome Research Limited	http://www.htslib.org/
Burrows-Wheeler aligner (B.W.A.)	Li H. ans Durbin R. 2009	http://bio-bwa.sourceforge.net/
MatLab R2018a	MathWorks Inc.	https://it.mathworks.com/products/matlab.html
Analyst 1.6.1 Software	AB Sciex Pte.Ltd.	https://sciex.com/

RESOURCE AVAILABILITY

Lead Contact

Further information and requests for resources and reagents may be directed to and will be fulfilled by the lead contact, Giovanni Roti (giovanni.roti@unipr.it).

Materials Availability

All unique/stable reagents generated in this study are available from the lead contact with a completed material transfer agreement.

EXPERIMENTAL MODEL AND SUBJECT DETAILS

Animals

NOD-*scid* IL2Rgamma^{null} (NSG) mice (The Jackson labs, RRID*:* IMSR_JAX:005557) for efficacy studies were maintained in specific pathogen–free facilities at the ''Preclinical Research Services Center'' (Ce.Se.R.P) at the University of Perugia (08/2018-UT of 07/24/2018). Animal procedures were approved by the University of Perugia IACUC following the DL 26/2014 and 2010/63/EU guidelines for the protection of animals used for scientific purposes. Pharmacokinetics (PK) and tolerability studies were performed at Aurigene Discovery Technologies, India. In-house breed CD1 (ICR) or BALB/cAnNCr mice for pharmacokinetics (PK) and tolerability studies were maintained in individually ventilated cages at the Aurigene facility in Hyderabad in India.

To assess effect of CAD204520 on the cardiac mechanics, cardiomyocytes were isolated from 12-14 week-aged Wistar rats (Rattus norvegicus, Charles River Laboratory, RRID: RGD_13508588) of 362±5 g in weight. Animals were housed in a temperature-controlled room (22–24°C), with a 12 hours light cycle (light on from 7.00 AM to 7.00 PM) with unrestricted food and water supply. Experiments were performed under the Veterinary Animal Care and Use Committee of the University of Parma-Italy and conform to the National Ethical Guidelines of the Italian Ministry of Health (Prot. N° 614/2016-PR) and the Guide for the Care and Use of Laboratory Animals (National Institute of Health, Bethesda, MD, USA, revised 1996).

Yeast Cells

Saccharomyces cerevisiae RS72 yeast cells (ATCC #9763) for the biochemical ATPase assay were pre-cultured in 100 ml sterile SGAH medium (7.04 g/L yeast nitrogen base, 19.8 g/L galactose, 64 mg/L adenine, 64 mg/L histidine) for 3 days at 25C and 150 rpm. The pre-culture was transferred to 500 mL sterile SGAH medium and further incubated for 3 to 4 days. 100 mL from the cell culture was transferred to 1 L YPAD medium (10 g/L yeast extract, 20 g/L bacto-peptone, 20 g/L glucose, 20 mg/L adenine) and incubated at 25C for 18-20 hours.

Cell Lines

Human cell lines DND41 (source: male), MOLT16 (source: female), REC-1 (source: male), Mino (source: female), PF382 (source: female), RPMI-8402 (source: female), SKW-3/KE-37 CTV-1 (source: male), HBS2 (source: male), Loucy (source: female) and PEER (source: female) were purchased from Leibniz-Institut DSMZ-German collection of microorganisms and cell cultures (Germany); the identity of ALL/SIL (source: male) was confirmed by PCR sequencing for known *NOTCH1* mutations and short tandem repeat (STR) loci profiling and they were kindly provided by Stegmaier laboratory. MAVER-1 (source: male) cells were a gift from the Muraro laboratory (C.R.O. National Cancer Institute, Aviano, Italy). Cells were cultured in RPMI 1640 (Fisher Scientific, Waltham MA, USA #MT10040CV) with 10% or 20% fetal bovine serum (FBS) (Thermo Fisher Scientific, Waltham MA, USA, Waltham MA, USA, #10270-106) and 1% penicillin-streptomycin (Fisher Scientific, Waltham MA, #3MT30002CI) and incubated at 37°C with 5% CO_2. 293T (source: human primary embryonal kidney cell line 293 (ACC 305)) cells were purchased Leibniz-Institut DSMZ-German collection of microorganisms and cell cultures (Germany) and cultured in DMEM (Fisher Scientific, Waltham MA, USA #11965-084) with 10% FBS and 1% penicillin-streptomycin and incubated at 37°C with 5% CO_2. HL-1 cardiac muscle cell line was a kind gift from the Miragoli laboratory (University of Parma, Parma, Italy). HL-1 cells were plated on a gelatin layer derived from bovine skin/fibronectin (1mg/ml)(Sigma-Aldrich, St. Louis, MO, USA, #G9391 and #F-1141) coated T25 flask and cultured in Claycomb medium (Sigma-Aldrich, St. Louis, MO, USA, #51800C) with 10% FBS, 1% penicillin-streptomycin, 2mM L-Glutamine (Thermo Fisher

Data Collection	
No. of data sets combined	2
Wavelength (A)	0.97625
Space group	P 41 21 2
Unit cell Dimensions (A)	a = 71.63 b = 71.63 c = 588.31
Resolution (A) [a]	58.83 - 3.40 (3.67 - 3.40)
No. unique reflections [a]	22,672 (4,468)
I/σI [a]	9.3 (1.6)
CC (1/2) [a]	100 (65.2)
R_{pim} (%) [a]	7.7 (77.9)
Completeness (%) [a]	100 (100)
Multiplicity [a]	36.6 (32.2)
Refinement	
Resolution (A)	54.52 - 3.40
No. reflections (refinement)	22,530
No. reflections (R-free)	1,138
R_{work} / R_{free} (%)	22.81 / 25.54
No. atoms	7749
Protein	7671
TNP-ATP	46
CAD204520	31
K^+	1
Average B-factors (A^2)	
Protein	118.07
TNP-ATP	155.59
CAD204520	130.33
K^+	138.60
R.m.s. deviations	
Bond lengths (A)	0.003
Bond angles (°)	0.72
Ramachandran	
favored / allowed / outliers (%)	90.32 / 8.97 / 0.71

[a]values in parentheses refer to the highest resolution shells as indicated

Scientific, Waltham MA, USA, Waltham MA, USA, #25030081), 0,1mM Norepinephrine [(±)- Arterenol] plus L-Ascorbic acid, sodium salt (Sigma-Aldrich, St. Louis, MO, USA, #A0937 and #A7506) and incubated at 37°C with 5% CO_2. Cytogenetic, FISH and mutation analysis was completed according to validated methods as previously described (La Starza et al., 2014, 2016).

Primary Samples

T-ALL lymphoblasts were obtained from patients with leukemia under an approved protocol at the Parma University Hospital (n.18249/18/05/2017) and according to the declaration of Helsinki guidelines for the protection of human rights. Peripheral blood (PB), and bone marrow (BM) samples were collected at the time of diagnosis, and we retained samples with blasts >85%. Mononuclear cells were isolated by density gradient centrifugation using LSM-lymphocyte separation medium (Cappel™ MP Biomedicals, LLC, Ohio, USA #50494). Lymphocytes were isolated from peripheral blood mononuclear cell PBMC by using a CliniMACS Prodigy (Miltenyi Biotec, Bergisch Gladbach, Germany) and cultured for a short time using the same growth conditions described above.

DATA AND CODE AVAILABILITY

The model and structure factors for the SERCA-CAD204520 complex structure reported in this paper have been deposited in the Protein Data Bank: PDB: 6YAA.

METHOD DETAILS

Preparation, Crystallization and Structure Determination of the SERCA-CAD204520 Complex

Rabbit sarcoplasmic reticulum (SR) membranes containing SERCA were prepared from rabbit hind leg muscle as previously described (Andersen et al., 1985). Briefly, muscle tissue was dissected and minced in 10 mM KCl, 2.5 mM K_2HPO_4, 2.5 mM KH_2PO_4, 2 mM EDTA, followed by centrifugation at 4°C for 20 min and 6.400 x g, supernatant filtered and spun at 9.700 x g for 20 min. SR membranes were sedimented by a 60 min centrifugation at 47.800 x g at 4°C. Membranes were homogenised and washed successively with buffers B (1 M sucrose, 50 mM KCl), C (1 M KCl, 3.4 mM MgATP pH 7.0), D (50 mM KCl), and E (0.3 M sucrose, 5 mM Hepes pH 7.4). Finally, washed membranes were extracted twice with extraction buffer (0.3 M sucrose, 0.5 M KCl, 1 mM EDTA, 10 mM Tris, 0.01 mM $CaCl_2$, 1.25 mM $MgCl_2$, pH7.9, 0.5 mg/ml DOC, 0.5 mg/ml DTT) followed by centrifugation at 4°C and 181.000 x g for 75 min. The pellet was then washed with 5 mM TAPS pH 7.5, 0.3 M sucrose, 0.5 M KCl, 0.5 mM $MgCl_2$, 10 μM $CaCl_2$, and finally resuspended and flash frozen in buffer E. SERCA membranes were resuspended and gently homogenized in 100 mM MOPS-Tris pH 6.8, 80 mM KCl, 3 mM $MgCl_2$, 4 mM EGTA and 20% (v/v) glycerol. CAD204520 was added to the membrane preparation at a final concentration of 0.5 mM and incubated overnight at 4°C. The following day, 0.4 mM TNPATP were added and incubated for 15 minutes (min) prior to the solubilization of the protein with $C_{12}E_8$ at a detergent/protein ratio of 1.5:1 (w/w). After 10 min incubation and centrifugation (TLA-100.3 rotor, 50,000 rpm, 30 min, 4°C), the concentration of solubilized protein was usually 10–12 mg/mL. Co-crystallization of SERCA with CAD204520 was carried out using hanging drop equilibration at room temperature (RT) with protein/buffer in a 1:1 ratio. The best diffracting crystals were obtained with crystallization buffer consisting of 10% glycerol, 14% PEG 6000, 100 mM NaCl and 6% MPD. Data were collected at 100 K and a wavelength of 0.976 A at beam line I03 at the Diamond Light Source (DLS) in Didcot, UK. The data were processed using XDS (Kabsch, 2010) and AIMLESS (Evans and Murshudov, 2013) and the structure was determined by molecular replacement in PHASER (McCoy, 2007) using a SERCA crystal structure with matching space group (pdb: 4UU0) (Drachmann et al., 2014). PHENIX (Adams et al., 2010) was used for refinement, ligand fitting and model validation and COOT for model building (Emsley and Cowtan, 2004). Figures were prepared with Pymol (Molecular Graphics System, Version 2.0 Schrödinger, LLC).

Synthesis Pathways

CAD307496 (2-[1-[3-(3-pyridyl)propyl]-2-piperidyl]-6-(trifluoromethoxy)-1H-indole) was prepared through the following intermediates:

(a) Intermediate 2-[2-(2-pyridyl)ethynyl]-5-(trifluoromethoxy)aniline: 2-Bromo-5-(trifluoromethoxy)aniline (6.21g, 24,2 mM), 2-ethynylpyridine (2.50g, 24.2 mM) and potassium carbonate (8.38g, 60.6 mM) in NMP (50 mL) were degassed with argon. Pd(DtBPF)Cl_2 (474mg, 0,73 mM) was added and the reaction heated under argon to 120℃ for 1 hour 45 min. The reaction cooled and diluted with water, extracted with 1:1 cHexane/EtOAc (3x 150 ml), washing each extract well with water. The combined extracts were dried, evaporated, and columned on 100 g SNAP cartridge eluting with 0-60% EtOAc/cHexane, using 20 column volumes to yield 750 mg of title compound as a brown solid. This was used without further purification.

(b) Intermediate 2-(2-pyridyl)-6-(trifluoromethoxy)-1H-indole: To 2-[2-(2-pyridyl)ethynyl]-5-(trifluoromethoxy)aniline (950mg, 3,41 mM) was added potassium 2-methylpropan-2-olate (383.13 mg, 3,41 mM) in DMF (50 mL) and the mixture was stirred at RT overnight. The reaction was quenched with 0.4 mL HOAc concentrated in vacuo, dissolved in diethyl ether and washed with sat. $NaHCO_3$ and water. The organic phase was dried, evaporated, columned on 50 g SNAP cartridge eluting with 20-60% DCM/cHexane using 20 column volumes to yield 510 mg of the title compound as a yellow solid.

(c) Intermediate A (2-(2-piperidyl)-6-(trifluoromethoxy)-1H-indole): 2-(2-pyridyl)-6-(trifluoromethoxy)-1H-indole (4.18 g, 15,02 mM) in ethanol (100 mL) and 1M HCl in methanol (45 mL) hydrogenated over PtO_2 (300 mg, 1.32 mM) at RT and pressure on 9.35. The mixture was warmed after 1 hour to 40℃ and left overnight after which additional PtO_2 (300 mg, 1.32 mM) was added and the reaction was stirred for another 5 hours. The catalyst was removed by filtration, and the filtrate evaporated to a white solid foam. This was taken up in DCM, and crystallized upon standing. The solid was broken up with diethyl ether and filtered to yield 3.7 g of title compound. The product may be converted to the hydrochloride by standard methods known to those skilled in the art.

(d) Intermediate 3-(3-bromopropyl)pyridine: To a stirring solution of 3-(3-pyridyl)propan-1-ol (0.14 g, 1 mM) in dichloromethane (2 mL) at 0℃ was added carbon tetrabromide (0.5 g, 1,5 mM) then triphenylphosphine (0.42 g, 1,6 mM) portion wise, carefully. The reaction mixture was then stirred at 0℃ for 2 hours. The material was applied to a DCM-wetted 5g SCX-2 cartridge; washed with DCM then eluted with 0.5 M DIPEA in DCM to yield a pink solution used in the next step.

(e) To 2-(2-piperidyl)-6-(trifluoromethoxy)-1H-indole hydrochloride (100 mg, 0,31 mM) was added 3-(3-bromopropyl)pyridine (10 mL, mixture of the bromide and DIPEA in DCM and prepared described above; 0.34 mM). The reaction mixture was stirred at RT for 1 hour and then left to stand overnight. The reaction mixture was heated at 45℃ and the DCM allowed to evaporate to concentrate the mixture after which DMF (1 mL) and DIPEA were added. A MDAP purification returned 35 mg of gum-like material which was run through a 2g SCX-2 cartridge yielding the title product after evaporation in 29 mg (23%) with satisfactorily purity. QC-LC-MS (99.2%). LC-MS (ESI): (M+H)+ = 404.1.

Intermediate A was used to produce additional compounds in a fashion similarly to that used in the preparation of CAD307496.

CAD204522

From Intermediate A and commercially available 4-(2-Chloroethyl)morpholine (CAS 3240-94-6). Yield 61%. QC-LCMS (ESI): (m/z) (M+H)+ = 398.1, (M-H)- = 396.3.

CAD204521

Intermediate A and commercially available 4-bromobenzaldehyde (CAS 1122-91-4) was added followed by HOAc (0.02 ml, 0.35 mM) and sodium triacetoxyborohydride (74.55mg, 0.35 mM). The reaction mixture was stirred for 1 hour and run through a MeOH-wetted SCX-2 cartridge, washed with methanol, and then eluted with 2M NH3 (aq). Yield 28%. QC-LCMS (ESI): (m/z) (M+H)+ = 453.0, (M-H)- = 451.1.

CAD204631

(3-(2-{1-[(4-bromophenyl)methyl]piperidin-2-yl}-6-(trifluoromethoxy)-1H-indol-3-yl)propan-1-ol): Intermediate 5-(2-pyridyl)pent-4-yn-1-ol: To 2-bromopyridine (2g, 12.7 mM), bis-triphenylphosphine palladium dichloride (1.1g, 1,58 mM) and CuI (301 mg, 1,58 mM) in triethylamine (50 mL, 358,7 mM) under argon was added dropwise pent-4-yn-1-ol (3.53 mL, 38 mM) and the mixture was heated to 50℃ for 21.5 hours after which the reaction was cooled, evaporated almost to dryness, and then partitioned between water and ethyl acetate. The phases were separated and the aqueous phase extracted with ethyl acetate. The combined organics were dried (sodium sulfate), filtered, and evaporated. The crude product was purified by column chromatography (Isolera, 100 g column; 0-100% ethyl acetate in cyclohexane to provide 3.98 g (78%) of the title product as a yellow liquid.

(a) Intermediate 3-[2-(2-pyridyl)-6-(trifluoromethoxy)-1H-indol-3-yl]propan-1-ol: 5-(2-Pyridyl)pent-4-yn-1-ol (3.98 g, 24,7 mM), 2-bromo-5-(trifluoromethoxy)aniline (6.32 g, 24.7 mM), potassium carbonate (8.53 g, 61.7 mM) and Pd(DtBPF)Cl_2 (805 mg, 1.23 mM) in 1-methyl-2-pyrrolidinone (100 mL) were degassed then heated at 120℃ under argon for 18 hours. The reaction mixture was split in two and each fraction passed through a MeOH-wetted SCX-2 cartridge (70 g); which were washed with methanol and then eluted with 2M ammonia in methanol. The ammonia fractions were evaporated and the crude product (8.3 g) was further purified on a Isolera (330 g column; 0-100% ethyl acetate in cyclohexane to yield 4.47g (54%) in accordance with the title compound.

(b) Intermediate B (3-[2-(2-piperidyl)-6-(trifluoromethoxy)-1H-indol-3-yl]propan-1-ol): A solution of 3-[2-(2-pyridyl)-6-(trifluoromethoxy)-1H-indol-3-yl]propan-1-ol (2.76 g, 8,21 mM) and PtO_2 (200 mg, 0,880 mM) in ethanol (100 mL) and 1M HCl in MeOH (24.62 mL, 24,62 mM) was degassed before placing under a H_2 atmosphere at RT for 4.5 hours. The reaction mixture was filtered through celite, the filterpad washed with additional ethyl acetate after which the filtrate was evaporated to give 4.02 g of a brown oil. The crude product was purified columned on Isolera (100 g column; 0-10% (2N ammonia in methanol) in DCM) to provide 2.48 g (88%) of a brown solid consistent with the title structure.

(c) From Intermediate B and commercially available 4-bromobenzaldehyde (CAS 1122-91-4) and a procedure similar to CAD204521. Yield 78%. QC-LCMS (ESI): (m/z) (M+H)+ = 511.1, (M-H)- = 509.1.

CAD204520

(4-[2-[2-[3-propyl-6-(trifluoromethoxy)-1H-indol-2-yl]-1-piperidyl]ethyl]morpholine) dihydrochloride was prepared through following intermediates:

(a) Intermediate 2-Pent-1-ynylpyridine: A slurry of 2-bromopyridine (8 g, 50.63 mM) and pent-1-yne (4.14 g, 60.76 mM) in triethylamine (141.16 mL, 1012.7 mM) degassed with argon added bis-triphenylphosphine palladium dichloride (1776.96 mg, 2.53 mM) and CuI (964.3 mg, 5.06 mM) was warmed to 50℃ overnight. The reaction mixture was diluted with diethyl ether and washed with water. The crude product was dried and evaporated, columned on 100 g SNAP cartridge eluting with 0-20% EtOAc/cHexane, using 15 column volumes to yield a black oil which was used without further purification.

(b) Intermediate 3-Propyl-2-(2-pyridyl)-6-(trifluoromethoxy)-1H-indole: 2-Bromo-5-(trifluoromethoxy) aniline (3879 mg, 15.15 mmol), 2-pent-1-ynylpyridine (2200 mg, 15.15 mM) and potassium carbonate (5235 mg, 37.88 mM) in NMP (20 mL) were degassed with argon. Pd(dtbpf)Cl_2 (494 mg, 0.760 mmol) was added and the reaction heated under argon to 120℃ overnight. The reaction mixture was then diluted with water, extracted with 1:3 EtOAc/cHexane, and subsequently diethyl ether. The combined extracts were dried, evaporated and columned on 100 g SNAP cartridge eluting with 0-10% EtOAc/cHexane to yield 2.225 g of product.

(c) Intermediate E: (2-(2-Piperidyl)-3-propyl-6-(trifluoromethoxy)-1H-indole hydrochloride): 3-Propyl-2-(2-pyridyl)-6-(trifluoromethoxy)-1H-indole (2.23 g, 6.95 mM) in ethanol (50 mL) and 1M HCl in methanol (21 mL) was hydrogenated over PtO2 (450 mg, 2.00 mM) at 40℃ for 7 hours after which the reaction mixture was left overnight at RT, in a hydrogen atmosphere. The reaction mixture was filtered, evaporated and taken up in 20 mL DCM. A white precipitate formed when 50 mL diethyl ether was added to give after drying 1.066 g (42%) of product. The mother liquor was columned after evaporation on a SNAP (50g) cartridge eluting with 0-10% NH3 in MeOH/DCM, using 15 column volumes. Fractions containing products were combined and evaporated to dryness to yield 0.544 g (23%) of title compound as the free base providing a combined yield of 66%.

(d) 4-[2-[2-[3-propyl-6-(trifluoromethoxy)-1H-indol-2-yl]-1 piperidyl]ethyl]morpholine dihydrochloride: 2-(2-Piperidyl)-3-propyl-6-(trifluoromethoxy)-1H-indole (140 mg, 0.430 mM), 4-(2-chloroethyl)morpholine hydrochloride (87.81 mg, 0.470 mM) and sodium bicarbonate (108.11 mg, 1.29 mM) in methyl alcohol (2 mL) was refluxed under argon for 75 min. The reaction mixture was filtered and concentrated, loaded onto an elute 5 g cartridge and eluted with EtOAc, then 5% MeOH/DCM. The crude

product was further purified by Xselect CSH 5 micron C18 prep column (19x250 mm) HPLC eluting with 10-60% MeCN/water (+0.1% HCO2H) to yield a product which was taken up in MeCN, 1M HCl (aq) and freeze dried to yield a white solid, 70 mg (31%) QC-LCMS (ESI): (m/z) (M+H)+ = 440.2, (M-H)- = 438.2.

CAD204519

From Intermediate E and commercially available 4-bromobenzaldehyde (CAS 1122-91-4) and a procedure similar to CAD204521. Yield 26%. QC-LCMS (ESI): (m/z) (M+H)+ = 495.0 (M-H)- = 493.1.

CAD306750

(1-{[(4-fluorophenyl)methyl]amino}-3-{2-[3-propyl-6-(trifluoromethoxy)-1H-indol-2-yl]piperidin-1-yl}propan-2-ol):

(a) Intermediate F: 1-Chloro-3-[2-[3-propyl-6-(trifluoromethoxy)-1H-indol-2-yl]-1-piperidyl]propan-2-ol: 2-(Chloromethyl)oxirane (163 mg, 1,76 mM) was dissolved in dichloromethane (1mL) and methyl alcohol (0.5 mL) and 2-(2-piperidyl)-6-(trifluoromethoxy)-1H-indole (Intermediate E, 500mg, 1.76mmol) was added. The reaction mixture was stirred at RT for 19 hours after which the reaction mixture was evaporated and columned on the Isolera (50 g cartridge, 0-5% (2N ammonia in methanol) in DCM) (yield 74%).

(b) Intermediate (1-{[(4-fluorophenyl)methyl]amino}-3-{2-[3-propyl-6-(trifluoromethoxy)-1H-indol-2-yl]piperidin-1-yl}propan-2-ol): From Intermediate F and commercially available 4-fluorobenzylamine (CAS 140-75-0) and sodium iodide (25.9 mg, 0.17 mM) in N,N-dimethylformamide (1mL) was heated at 70℃ for 22 hours after which the reaction was poured into water and extracted with EtOAc. The organic phases were dried (sodium sulfate), filtered and evaporated. The crude material was purified using Isolera column chromatography (0-10% (2N ammonia in methanol) in DCM). The crude product was further purified using preparative HPLC (C18, Xselect, 20-80% MeCN in water plus 0.1% formic acid). Yield 33%. QC-LCMS (ESI): (m/z) (M+H)+ = 508.1, (M-H)- = 506.2. The product is a 1:1 mixture diastereomer.

CAD306749

This compound was produced in a similar way as CAD306750 from Intermediate F and commercially available 1-(3-Bisphenylyl) methanamine (CAS 177976-49-7). Yield 19%. QC-LCMS (ESI): (m/z) (M+H)+ = 566.2 (M-H)- = 564.2

CAD305666

(2-[2-[1-[(4-bromophenyl)methyl]-2-piperidyl]-6-(trifluoromethoxy)-1H-indol-3-yl]ethanol):

(a) Intermediate 2-[2-(2-pyridyl)-6-(trifluoromethoxy)-1H-indol-3-yl]ethanol: Was prepared similar to CAD204631 step (a). Yield 52%.

(b) Intermediate 2-[2-(2-piperidyl)-6-(trifluoromethoxy)-1H-indol-3-yl]ethanol was prepared similar to intermediate B (step (b) for CAD204631) Yield 45%.

(c) Intermediate 2-[2-[1-[(4-bromophenyl)methyl]-2-piperidyl]-6-(trifluoromethoxy)-1H-indol-3-yl]ethanol was obtained using Intermediate 2-[2-(2-piperidyl)-6-(trifluoromethoxy)-1H-indol-3-yl]ethanol and commercially available 4-bromobenzaldehyde (CAS 1122-91-4) and a procedure similar to CAD204521. Yield 87%. QC-LCMS (ESI): (m/z) $(M+H)^+$ = 497.1 (M-H)- = 495.1.

CAD204630

(2-[1-[(4-bromophenyl)methyl]-2-piperidyl]-3-isopentyl-6-(trifluoromethoxy)-1H-indole hydrochloride):

(a) Intermediate 3-isopentyl-2-(2-pyridyl)-6-(trifluoromethoxy)-1H-indole: By a method similar to that of CAD204631 step (a) above using commercially available 2-Bromo-5-(trifluoromethoxy)aniline (CAS 887267-47-2) and 2-(5-methylhex-1-ynyl)pyridine. Yield 60%.

(b) Intermediate 3-isopentyl-2-(2-piperidyl)-6-(trifluoromethoxy)-1H-indole: By a method similar to intermediate B (step b for CAD204631). Yield 56%.

(c) 2-[1-[(4-bromophenyl)methyl]-2-piperidyl]-3-isopentyl-6-(trifluoromethoxy)-1H-indole hydrochloride: By a method similarly to that of CAD204521 employing commercially available 4-bromobenzaldehyde (CAS 1122-91-4). Yield 62%. QC-LCMS (ESI): (m/z) $(M+H)^+$ = 523.1 $(M-H)^-$ = 521.1. Note: Many of the compounds are racemates i.e. of enantiomers or diastereomers. The pure enantiomer was not isolated.

ATPase Preparation

Heat competent *Saccharomyces cerevisiae* RS72 yeast cells (Cid et al., 1987) were transformed using a lithium acetate, single-stranded carrier DNA/polyethylene glycol method and with a yeast multicopy vector (Hill et al., 1986) containing the full-length cDNA of the *S. cerevisiae* plasma membrane H^+-ATPase isoform *PMA1* under control of the *PMA1* promoter. Transformed yeast cells were pre-cultured in 100 mL sterile SGAH medium (7.04 g/L yeast nitrogen base, 19.8 g/L galactose, 64 mg/L adenine, 64 mg/L histidine) for 3 days at 25℃ and 150 rpm. The pre-culture was transferred to 500 mL sterile SGAH medium and further incubated for 3 to 4 days. 100 mL from the cell culture was transferred to 1 L YPAD medium (10 g/L yeast extract, 20 g/L bacto-peptone, 20 g/L glucose, 20 mg/L adenine) and incubated at 25℃ for 18-20 hours. Recombinant yeast was harvested by 2-3 min of centrifugation at 3.000 x g and 4℃, followed by 2 times wash in milli-Q water. Harvested cells were incubated in 10% glucose for 10 min, on a shaking table, and centrifuged at 3.000 x g and 4℃. Cells were re-suspended in homogenisation buffer (50 g/L glucose, 28.3% glycerol, 0,1 M Tris-HCl

pH 7.25, 10 mM EDTA pH 8.0, 50 mM KCl, 1mM DTT, 200 μM PMSF, 2 μg/ml Pepstatin A), and disrupted with 165 g glass beads (500 μm) by runs in a BeadBeater (Biospec). The disrupted cells were centrifuged at 4°C for 5 and 15 min at 1.400 x g and 12.000 x g, respectively. The supernatant was collected and centrifuged at 251.000 x g for 1 h with 112 μM phenylmethylsulfonyl fluoride (PMSF) and 1.1 μg/mL Pepstatin A. The resulting pellet was re-suspended in $GTEK_{20}$ buffer (20% glycerol, 10 mM Tris-HCl pH 7.25, 25 mM KCl, 0.5 mM EDTA pH 8.0, 1 mM DTT, 0.2 mM PMSF, 2 μg/ml Pepstatin A) and centrifuged for 45 min at 251.000 x g and 4°C. Pellet was then re-suspended in $STKED_{20}$ buffer (200 g/L sucrose, 40 g/L glucose, 50 mM Tris-HCl pH 7.25, 50mM KCl, 1 mM EDTA pH 8.0, 1 mM DTT, 0.2 mM PMSF, 2 μg/ml Pepstatin A), homogenised and diluted with $STKED_{20}$ buffer. The plasma membranes were recovered at the interface of a 43%/53% (wt/wt) step sucrose gradient containing sucrose in 50 mM Tris-HCl pH 7.25, 50 mM KCl, 1 mM EDTA, 1 mM DTT. Centrifugation was done for 16 h at 154.000 x g and 4°C. The plasma membrane fraction was collected and diluted with $GTEK_{20}$ buffer and centrifuged for 1 hour at 274.000 x g. Pellet was collected and homogenised in $GTEK_{20}$ buffer and stored at -80°C.

Sarco/Endoplasmic reticulum (SR) Ca^{2+}-ATPase was provided in SR membranes purified by extraction with a low concentration of deoxycholate (DOC) as described above. The pig kidney Na^+/K^+-ATPase purification included a mild SDS treatment of isolated microsomes followed by a washing step and was kindly performed by Natalya Fedosova, Aarhus University and prepared as described in (Klodos et al., 2002). In brief, pieces of outer medulla were extracted and cut in pieces and further suspended and homogenized in ISE-buffer (25 mM imidazole, 250 mM sucrose, 1 mM EDTA pH 7.4). Microsomes were isolated by differential centrifugations. The final pellet was suspended and homogenized in ISE-buffer and stored at -20°C.

ATP Hydrolysis Inhibition

ATPase activity was determined by measuring the amount of liberated phosphate from ATP hydrolysis. The ATPase assay was performed in 96 well plates in a final reaction volume of 60 μL. 0.1-0.2 μg/well of DOC extracted SERCA membrane or the Na^+/K^+-ATPase was used, while 1-2.5 μg/well was used of the Pma1 membrane preparation. Reactions including protein membrane preparation and exogenously added compounds in a ½ log dilution concentration range from 333 μM or 166 μM to 0.005 μM. We conducted the enzymatic reactions in the following buffers; Pma1 buffer: 17.5 mM MOPS-NaOH pH 7, 7 mM $MgSO_4$, 44 mM KNO_3 (vacuolar ATPase inhibitor), 22 mM NaN_3 (mitochondrial ATPase inhibitor), 0.22 mM Na_2MoO_4 (acid phosphatase inhibitor); SERCA buffer: 9 mM MOPS-NaOH pH 7, 2.7 mM $MgCl_2$, 0.1 mM $CaCl_2$ and 72 mM KCl. Na^+/K^+-ATPase buffer: 30 mM MOPS-NaOH pH 7, 40 mM NaCl, 4 mM $MgCl_2$ and 20 mM KCl. Reactions were started by the addition of Na-ATP to a final concentration of 2.5 mM (Pma1 and Na^+/K^+-ATPase) or 5 mM (SERCA), followed by 30 min incubation at 30°C. The amount of liberated phosphate was determined calorimetrically after addition of STOP solution (mixture of L-ascorbic acid, ammonium heptamolybdate tetrahydrate, and HCl to give final concentrations of 65 mM, 2.2 mM, and 189 mM, respectively) with 5 min incubation at RT followed by addition of arsenite solution (mixture of $NaAsO_2$, sodium citrate dihydrate, and acetic acid to give final concentrations of 3.1 mM, 28 mM, and 141 mM, respectively). We measured absorption at 860 nm after additional 30 min incubation at RT.

Cell Viability, Apoptosis and DNA Content Assays

ATP-based cell viability was determined using the CellTiter-Glo viability assay (Promega Corporation, Madison, WI, USA #G7573) and luminescence was measured using a Victor X4 (Perkin Elmer, Waltham, MA, USA). Apoptotic rate was quantified by staining cells with Annexin V and propidium iodide using a flow-cytometry commercial kit (eBioscience™ Annexin V Apoptosis Detection Kit APC, Waltham MA, USA, # 88-8007-74). Cells were analyzed by flow cytometry with a FACScan flow cytometer (Beckman Culture-Cytomics FC 500, Life Sciences Division, Indianapolis, USA) and FlowJo V10 (Tree Star LLC, Ashland, OR, USA) analytical software. Cellular DNA content was assessed by staining with propidium iodide (50 g/mL) and analyzed by flow cytometry. At least 20,000 events were acquired and all determinations were replicated at least twice.

Cell Competition Assay

SKW-3/KE-37-GFP and MOLT16 were co-cultured at 1:1 ratio in RPMI 1640, 10% FBS, 1% P/S medium. 1 x 10^6 cells per condition were treated with CAD204520 at the following concentrations 2.5 and 5 μM and DMSO at 0.005% and 0.01% respectively and incubated at 37°C. After 72 hours, T-ALL cells were washed in PBS, and stained with a LIVE/DEAD Fixable Far Red Dead Cell Stain (Invitrogen, Life Technologies, Carlsbad, CA, USA, #L34973) for 30 min. Fluorescent signal was assessed by flow-cytometry [Beckman Culture-Cytomics FC 500 (Life Sciences Division, Indianapolis, USA) and FlowJo V10 (Tree Star LLC, Ashland, OR, USA) analytical software]. A minimum of 20,000 events was collected for each biological sample. Experiments are representative of two independent experiments.

Compound Sources

We obtained the compounds for this study from the following sources: DAPT (N-[N-(3,5-difluorophenacetyl)-1-alanyl]-(S)-phenylglycine) (Selleckchem, Houston, TX USA, #S2215), thapsigargin (Enzo Biochem, Inc., USA #BML-PE180-0005).

Compound Treatment of Cell Lines and Primary Cells

Cells were seeded in 384-well plates (Corning Life Sciences Plastic, Bedford MA, USA, #3570) at the final concentration of 0.02 x 10^6/mL per condition. Small molecules were added with a nanometric dispenser Tecan D300e (Tecan Trading AG, Switzerland), and

cellular viability was assessed after 72 hours of drug treatment using a CellTiter-Glo ATP assay (Promega Corporation, Madison, WI, USA, #G7573). IC_{50} and the area under the curve (AUC) were calculated using GraphPad Prism software (La Jolla, CA, USA).

Intracellular Calcium Measurement

Cytosolic Ca^{2+} concentration was measured using the Indo-1 AM probe (ThermoFisher Scientific, Waltham MA, USA, #I1223). Cells were washed twice with a calcium free solution (D-PBS Life Technologies, Carlsbad, CA, USA, #10010015) and loaded at 37°C in 5% CO_2 for 30 min with 5 μM of Indo-1 AM. Then, cells were washed twice with D-PBS and equilibrated in RPMI 1640 (Thermo Fisher Scientific, Waltham MA, USA, Waltham MA, USA #MT10040CV) with 10% FBS (Sigma-Aldrich, St. Louis, MO, USA, #F2442-500ML) and 1% penicillin-streptomycin (Thermo Fisher Scientific, Waltham MA, USA, #3MT30002CI) for 5 min at 37°C. Baseline fluorescence of Indo-1 AM loaded cells was acquired for 1 min LSR Fortessa X20 flow cytometer (BD Biosciences, San Jose, CA, USA). Subsequently DMSO (0.1%), CAD204520 1 μM, or thapsigargin 1 μM were added and measurement was resumed for a total of 10 min. Data analysis was performed using FlowJo V10 (Tree Star LLC, Ashland, OR, USA) analytical software.

ER Ca^{2+} release and re-uptake was measured with the IonOptix system (IonOptix, Milton, MA, USA). Ca^{2+} signals were detected by epifluorescence after loading T-ALL cells (ALL/SIL, DND41) with Fluo-3-AM (10 μM; Invitrogen, Carlsbad, CA, USA) in PBS (Gibco, Thermo Fisher Scientific, Waltham, MA, USA) for 20 min, at RT. After removing the fluorophore, cells were washed with PBS for 30 min and then placed ($1x10^6$; 1ml volume) in a chamber mounted on the stage of an inverted microscope (Nikon-Eclipse TE2000-U, Nikon Instruments, Florence, Italy). The recording started with measurement of baseline fluorescence. Then, 1 μM CAD204520, 1 μM thapsigargin, or DMSO (0.1%) were manually added with a pipette, and the recording was continued for up to 15 min (during the first 7 min: 5 seconds of recording followed by 5 seconds of rest; in the remaining 8 min: 5 seconds of recording followed by 30 seconds of rest). Excitation length was 480 nm, with emission collected at 535 nm. The following parameters were evaluated: (i) peak fluorescence normalized to baseline fluorescence (f/f0_peak), (ii) time at 50% of fluorescence signal decay, measured from the peak time (time_50%-f/f0), and normalized fluorescence computed at 3, 5, and 10 min from the peak time (f/f0_3min, f/f0_5min, and f/f0_10 min).

Western Blot

Protein lysates for western blotting were incubated with antibodies specific for γ-secretase-cleaved NOTCH1 (Val1744, #4147 or #2421 Cell Signaling, Beverly, MA, USA) or the C-terminus of NOTCH1 (#SC-6014 (C-20), Santa Cruz Biotechnology, Santa Cruz, CA, USA). Cleaved form of Poly (ADP-ribose) polymerase was detected using an antibody specific for the cleaved peptide of PARP (#9541, Cell Signaling, Beverly, MA, USA). The expression of SERCA isoforms in ALL/SIL were detected using SERCA2 (#9580, Cell Signaling, Beverly, MA, USA) and SERCA3 (#sc-81759, Santa Cruz Biotechnology, Santa Cruz, CA, USA) antibodies. Loading controls were performed with antibodies specific for β-Actin, (#BK3700S, Cell Signaling, Beverly, MA, USA), GAPDH (#137179, Santa Cruz Biotechnology, Santa Cruz, CA, USA) or HSP90 (# sc-69703 (4F10)), Santa Cruz Biotechnology, Santa Cruz, CA, USA). Effects on the endoplasmic reticulum stress pathway (ER stress) we used the following antibodies: BiP, (#BK3177S), phospho-eIF2α (Ser51) (#9721S), eIF2α (#9722S) (Cell Signaling, Beverly, MA, USA). Blots were developed using species specific fluorescent antibodies obtained from LI-COR (Biosciences, Lincoln, NE, USA) such as IRDye 680LT Goat anti-Mouse IgG (#925-68020); IRDye 800CW goat anti-rabbit IgG (#925-32211); IRDye 680RD goat anti-rabbit IgG (#925-68071). Cell surface NOTCH1 was evaluated by staining non-permeabilized cells with monoclonal anti-human NOTCH1 antibody (#FAB5317P, R&D, Minneapolis, MN, USA).

Indirect Immunofluorescence Microscopy

DND41, REC-1 and ALL/SILL cells were resuspended in PBS, spotted on immunofluorescence slides (Thermo Fisher Scientific, Waltham, MA) by a cytospin centrifuge (CR2000, Small Prime Centrifuge, Centurion) fixed for 10 min in 4% paraformaldehyde (#28908, Thermo Fisher Scientific, Waltham MA, USA), permeabilized in 0.2% Triton X-100 for 5 min, and blocked in 5% bovine serum albumin for 1 hour. Then, the cells were incubated with primary antibodies against full length NOTCH1 (#SC-6014 (C-20) Santa Cruz Biotechnology, Santa Cruz, CA, USA or #ab44986 (A6) Abcam, Cambridge, United Kingdom), GOLGA1 (#SAB1409131, Sigma-Aldrich, St. Louis, MO, USA), and ATF6 (#37149, Abcam, Cambridge, United Kingdom).

Alexa Fluor 488 (#A11029, Invitrogen, Carlsbad, CA, USA) and Alexa Fluor 568 (#A11036, Invitrogen, Carlsbad, CA, USA) were used as secondary antibodies and cells were incubated 1 hour at RT protected by the light. Nuclei were stained with DAPI (#D9542, Sigma-Aldrich, St. Louis, MO, USA). Coverslips were mounted with Prolong Gold Antifade reagent (#P36934, Thermo Fisher Scientific, Waltham MA, USA). Images were captured using a EVOS FL microscope (Thermo Fisher Scientific, Waltham MA, USA) and analyzed using ImageJ software (http://rsbweb.nih.gov/ij/).

Real-time RT-PCR

Primers and probes for real-time RT-PCR were obtained from Applied Biosystems (Foster City, CA, USA) (*RPL13A* #Hs01926559_g1, *MYC* #Hs00153401_m1, *DTX1* #Hs00269995_m1). The data were analyzed using the ΔΔCT method and plotted as percentage of transcript compared to vehicle.

Whole Exome Sequencing

DNA was extracted from about 10 x 10^6 ALL/SIL o ALL/SIL thapsigargin resistant using a Promega Maxwell® kit as per the manufacturer's protocol (Promega Corporation, Madison WI, USA, #AS1010).

A total amount of 1.0 μg genomic DNA per sample was used as input material for the DNA library preparation. Sequencing libraries were generated using Agilent SureSelect Human all exon kit (Agilent Technologies, CA, USA) following manufacturer's recommendations and index codes were added to each sample. Briefly, fragmentation was carried out by hydrodynamic shearing system (Covaris, Massachusetts, USA) to generate 180-280bp fragments. Remaining overhangs were converted into blunt ends via exonuclease/polymerase activities and enzymes were removed. After adenylation of 3' ends of DNA fragments, adapter oligonucleotides were ligated. DNA fragments with ligated adapter molecules on both ends were selectively enriched in a PCR reaction. After PCR reaction, library hybridizes with liquid phase with biotin labeled probe, after which streptomycin-coated magnetic beads are used to capture the exons of genes. Captured libraries were enriched in a PCR reaction to add index tags to prepare for hybridization. Products were purified using AMPure XP system (Beckman Coulter, Beverly, USA) and quantified using the Agilent high sensitivity DNA assay on the Agilent Bioanalyzer 2100 system and sequenced with Hiseq PE 150 (Illumina®, San Diego, CA, USA). Paired-end clean reads were aligned to the reference genome (hg38) with Burrows-Wheeler aligner (B.W.A.). SAMtool was used to sort and index the original BAM files and Picard marked duplicates reads. Coverage and depth was calculated based on the final BAM files. If a read or reads pair were mapped to multiple positions, B.W.A. will choose the most likely position. If two or more likely position were present B.W.A. will choose one randomly. This multiple hit strategy has significant impact on SNP, INDEL and CNV detection, and variant calling accuracy. Following genomic variant detection, we performed annotation of variants with the tool ANNOVAR (Wang et al., 2010) in multiple aspects, including protein coding changes, affected genomic regions, allele frequency etc.

Virus Production and Transduction of T-ALL Cell Lines

3 x 10^6 293T were plated in 10 cm plates and maintained in DMEM media (Life Technologies, Carlsbad, CA, USA, #11965118), 10% FBS (Sigma-Aldrich, St. Louis, MO, USA, #F2442-500ML), 1% penicillin-streptomycin (Thermo Fisher Scientific, Waltham MA, #3MT30002CI) and incubated at 37°C with 5% CO^2, until sub confluent. Cells were transfected with 2 μg of pCMV-VSV-G envelope vector, Delta 8.9 packaging plasmid and pXPR-011-GFP, a vector expressing a green fluorescent protein (GFP), according to the FuGENE 6 protocol (Promega Corporation, Madison WI, USA, #E2691). The tissue culture medium was changed to RPMI 1640 24 hours post-transfection, and viral supernatant was harvested and filtered (0.2 μm) 48 hours post-transfection. 4 x 10^6 SKW-3/KE-37 T-ALL cells were resuspended in 100 μL of RPMI 1640 and spin-infected for 1 hour at 37°C with 100 μl lentivirus particles and 8 μg/mL polybrene (Sigma-Aldrich, St. Louis, MO, USA). Cells were selected 48 hours later with 1 μg/mL puromycin (Sigma-Aldrich, St. Louis, MO, USA).

Cardiomyocyte Isolation and Treatment

Individual left ventricular (LV) myocytes were enzymatically isolated by collagenase perfusion, following a procedure previously described (Meraviglia et al., 2018). Briefly, after sacrifice, the rat heart was rapidly removed, mounted on a Langendorff apparatus and perfused at 37°C with the following sequence of solutions: solution 1: calcium-free solution for 5 min containing the following (expressed in mM/L): 126 NaCl, 22 dextrose, 5.0 $MgCl_2$, 4.4 KCl, 20 taurine, 5 creatine, 5 Na pyruvate, 1 NaH_2PO_4, and 24 HEPES (pH = 7.4, adjusted with NaOH); solution 2: solution 1 plus 0.1 mM Ca^{2+}, 1 mg/ml type 2 collagenase (Worthington Biochemical, USA), and 0.1 mg/ml type XIV protease (Sigma, Milan, Italy) for about 15 min, and solution 3: solution 1 plus 0.1 mM Ca^{2+} (enzyme-free) for 5 min. All solutions were gassed with 100% O^2. Afterward, the LV was minced and shaken for 5 min. The cells were filtered through nylon net and re-suspended in the low calcium solution for 30 min, then slowly brought to a final calcium concentration of 1 mM (maintenance solution).

A total of 8 rats (male) were scarified for these experiments. Specifically, cardiomyocytes isolated from the heart of 6 rats were either untreated (Control group) or incubated with 5 μM CAD204520 for 2 hours ($CAD204520_{2hr}$) or 4 hours ($CAD204520_{4hr}$) and then used for recording cell mechanics (IonOptix, Milton, MA, USA) (Bocchi et al., 2018; Meraviglia et al., 2018). Cardiomyocytes isolated from additional 2 rats were incubated with thapsigargin, at two different concentrations, 200 nM or 500nM for 2 hours and then submitted to the same experimental protocol (Control number of cells n=63; $Thapsigargin_{200nM}$, n=28; $Thapsigargin_{500nM}$; n=25. Left ventricular myocytes were placed in a chamber mounted on the stage of an inverted microscope (Nikon-Eclipse TE2000-U, Nikon Instruments, Florence, Italy) and superfused (1 mL/min at 37°C) with a Tyrode solution containing (in mM): 140 NaCl, 5.4 KCl, 1 $MgCl_2$, 5 HEPES, 5.5 glucose, and 1 $CaCl_2$ (pH 7.4, adjusted with NaOH) (Sigma-Aldrich, Milan, Italy). The cells were field stimulated at a frequency of 0.5 Hz by constant current pulses (2 milli seconds in duration, and twice diastolic threshold in intensity; MyoPacer Field Stimulator, IonOptix). Load-free contraction of myocytes was measured with the IonOptix system, which captures sarcomere length dynamics via a Fast Fourier Transform algorithm. The following parameters were computed: mean diastolic sarcomere length, fraction of shortening (FS), and the maximal rates of shortening (-dl/dtmax) and re-lengthening (+dl/dtmax). Steady-state contraction of myocytes was achieved before data recording by means of a 10 seconds conditioning stimulation. Sampling rate was set at 1 kHz. In a fraction of cells from each experimental group, calcium transients were measured simultaneously with cell motion, after loading the myocytes with Fluo-3 AM (10 μmol/L; Invitrogen, Carlsbad, CA, USA) for 30 min. Excitation wavelength was 480 nm, with emission collected at 535 nm. Fluo3 signals were expressed as normalized fluorescence (f/f0: fold increase). The time course of the fluorescence signal decay was described by a single exponential equation, and the time constant (Tau) was used as a measure of the rate of intracellular calcium clearing. Only rod-shaped myocytes exhibiting cross striations and no spontaneous contractions were

selected for physiological measurements. Cardiomyocyte subgroups were washed three times with low-calcium solution and centrifuged (42 x g for 5 min). After removing the supernatant, the pellet was stored at −80°C for intracellular ATP content detection (as described below).

Intracellular ATP Content Detection

The intracellular content of ATP was measured by the luminescence ATP-lite assay (PerkinElmer, Waltham, MA, USA, #6016943) according to the manufacturer's protocol, using an EnSpire® multimode plate reader (PerkinElmer, Waltham, MA, USA). Briefly, a frozen pellet of cardiomyocytes (both untreated or incubated with 5 μM CAD204520 for 2 or 4 hours) was re-suspended in 1 mL of PBS, and then 20 μL of this suspension were further diluted 20 times in PBS. 100 μL of each diluted sample were lysed and assayed for ATP content in triplicate, as previously detailed (Bocchi et al., 2018). The row luminescence data were normalized for the total protein content measured by the DC Protein assay kit (Bio-Rad, Hercules, CA, USA).

In Vivo Studies

In brief 6 male, 7-9 weeks old CD1 (ICR) in-house breed mice (Aurigene, India) were treated with 30 mg/Kg/diem CAD204520 in fed state by oral gavage dissolved in Tween-80 0.5% w/v (Sigma-Aldrich, Missouri, USA) and hydroxypropyl-methylcellulose (HPMC) 1.0% w/v (Shin-Etsu Chemical Co., Tokyo, Japan) to model PK and biodistribution data. Samples from the plasma and brain were collected at eight time points (5 min to 24 hours). CAD204520 concentration was assessed by LC/MS-MS method and PK parameters (Tmax, Cmax, T1/2, AUC, etc.) were calculated with Analyst 1.6.1 software using a one-compartment model. Lambda Z PK parameters was reviewed by LD ADME consult (Copenhagen, Denmark) to model multiple doses PO infusion and time-concentration data. For tolerability studies, 6-8 weeks BALB/cAnNCr mice per group (3 male and 3 female) were treated BID with 30 mg/Kg CAD204520 or vehicle (see above) by oral gavage at 8 hours interval. CAD204520 and vehicle were administered from day 1 to day 21 by oral route. Daily body weight measurement before dosing and adverse events were recorded. Animals were sacrificed on day 21. In a subsequent experiment, 6 BALB/cAnNCr mice per group (3 male and 3 female) were treated with 30 mg/Kg CAD204520 (BID) for 7 days and for the remaining of the study (day 7 to day 21) with 60 mg/Kg (BID).

To generate NOTCH1-dependent T-ALL tumors in mice, 10 x 10^6 SKW-3/KE-37 cells were transplanted via the retro-orbital venous sinus in adult (10-12 weeks old) non-irradiated NSG mice (day 0) (Baldoni et al., 2018). Once disease was established at day 12 after transplant, animals were divided into two treatment groups of eight mice each (3 male and 5 female): vehicle [tween-80 0.5% w/v (Sigma-Aldrich, Missouri, USA) and hydroxypropyl-methylcellulose (HPMC) 1.0% w/v (Shin-Etsu Chemical Co., Tokyo, Japan)] or 30 mg/kg BID of CAD204520. Animals were treated with either vehicle or CAD204520 at 30 mg/kg BID (PO) for 4 days. Antileukemic activity of CAD204520 was assessed by measuring human $CD45^+$ expression (clone HI30, BD Biosciences, New Jersey, USA) on peripheral blood blast cells by flow cytometry (FACS CANTO, BD Biosciences, San Jose, CA, USA) and by quantification of $hCD45^+$ cells in formalin-fixed, paraffin-embedded spleen sections [(clones 2B11 + PD7/26 Dako, Agilent, Stevens Creek Blvd Santa Clara, CA, USA)]. Complete blood count was performed using an XE-2100 hematology automated analyzer (Dasit). Formalin-fixed, paraffin-embedded heart and gut sections were stained using hematoxylin and eosin. Images were acquired at different magnifications using a Leica DM750 microscope (Leica Microsystems, Wetzlar, Germany).

QUANTIFICATION AND STATISTICAL ANALYSIS

Assumption of normal distribution was not determined and *P*-value was calculated by non-parametric t-test (Mann-Whitney) by comparing treated samples to untreated controls. Significance across groups was determined by one-way or two-way ANOVA using Bonferroni correction for multiple comparisons testing when appropriate. Statistics were performed using GraphPad Prism software. Graphs show means and standard deviation (±SD) as indicated in the figure legends. Statistical significance, group size, and experimental details are described in the figure legends and/or in the Method Details.